

A dissertation submitted in partial fulfillment of the
requirements for the Master's Degree in Electrical
Engineering

Three-phase grid-forming droop control for unbalanced systems and fault ride through

Prajwal Bhagwat
Under the guidance of Prof. Dominic Groß

Aug 2023

Dept. ECE
University of Wisconsin, Madison

Contents

Acknowledgment	vi
Abstract	vii
1 Introduction	1
1.1 Motivation	1
1.2 Literature review	1
1.3 Outline	3
2 GFM converter setting	4
2.1 Topology	4
2.2 Connection on the dc side	4
2.3 Filter configuration	4
2.4 Measurements	5
2.5 Transformer	5
3 Coordinate frames	6
3.1 Signals	6
3.2 $dq0$ coordinates for balanced systems	6
3.3 Unbalanced systems	7
3.3.1 Symmetrical components	7
3.3.2 Hilbert transform	7
4 Converter control	9
4.1 General tasks	9
4.2 Standard (positive sequence) GFM control	10
5 Generalized three-phase GFM control	12
5.1 Control Overview	12
5.2 Control description	12
5.2.1 Generalized three-phase droop control	13
5.2.2 Dual-loop current/voltage control and current limiting	14
5.2.3 Discussion	16
6 Steady state analysis	17
6.1 Voltage magnitude and angle unbalances	17
6.1.1 $Q - V$ droop equation	17
6.1.2 $P - f$ droop equation	18

6.2	Unbalance factors	19
6.2.1	Linearizing voltage unbalance factor	19
6.2.2	Standalone GFM converter with unbalanced load	21
6.2.3	GFM converter connected to unbalanced grid	24
7	Case study	26
7.1	System description	27
7.2	Unbalanced load	27
7.3	Single line-to-ground fault	27
7.3.1	Current saturation algorithm (CSA)	28
7.3.2	Threshold virtual impedance (TVI)	32
7.4	IEEE 13-bus system	34
8	Conclusion	36

List of Figures

1.1	GFL converter acting as a current source (upper image), GFM converter acting as a voltage source (lower image).	2
2.1	GFM converter consisting of 2-level VSC with mid point dc grounding. Note that the filter is in star configuration with its neutral point connected to ground. The $\Delta\forall$ transformer is used to connect GFM converter to grid.	5
4.1	Standard dual-loop GFM control with inner controls tracking a positive sequence voltage reference provided by an outer GFM control (e.g., droop control [1], VSM [2]).	10
5.1	Generalized three-phase GFM control with inner control for every phase tracking a voltage reference provided by the outer GFM control (5.7) with phase balancing feedback.	13
5.2	Droop control structure of generalized three-phase GFM control.	14
5.3	Virtual impedance $Z_{VI} := R_{VI} + j\omega_p^{\text{gfm}} L_{VI}$ in the GFM control structure and effective impedance emulation.	15
5.4	Virtual impedance activation and control structure.	15
6.1	VSC of GFM converter is connected to an unbalanced load.	21
6.2	Constraint sets for the maximization of voltage unbalance factor.	23
6.3	VSC of GFM converter is connected to an unbalanced load.	24
7.1	Test system with a low-voltage VSC connected to a weak ac system through a distribution line, double circuit transmission line, and a step up transformer.	27
7.2	Steady-state unbalance factors for an unbalanced load at the VSC terminal and various phase balancing gains k_s	28
7.3	VSC voltages during a phase a to ground fault using generalized three-phase droop control with dual-loop current/voltage control for every phase (top) and standard droop control and dual-loop current/voltage control (bottom).	29
7.4	Critical clearing time vs phase balancing gain k_s for different SCR values. The vertical axis is critical clearing time mentioned in terms of ac cycles at nominal frequency.	30
7.5	Response of generalized droop control to a phase a to ground fault on a transmission line at $t = 1.5$ s with CSA current limiting. The fault is cleared after ten cycles by disconnecting the faulted line.	31

7.6	Resynchronization time vs phase balancing gain k_s . Dotted lines employ TVI for current limiting while solid lines employ CSA.	32
7.7	Response of generalized droop control to a phase a to ground fault on a transmission line at $t = 1.5$ s, with TVI current limiting. The fault is cleared after ten cycles by disconnecting the faulted line.	33
7.8	IEEE 13 bus distribution system with GFM converter. Fault is simulated on the indicated spot to determine existing inverse time relay (indicated in orange) responses.	34
7.9	ABC-g fault with inverse time relay. Graphs (a) (c) (e) indicate the response of Relay 1 and graphs (b) (d) (f) indicate the response of Relay 2 as per fig. 7.8.	35

List of Tables

7.1	Parameters used in the model illustrated in fig. 7.1	26
-----	--	----

Acknowledgment

Knowledge is an ever expanding universe, where the research is the process of creating new stars. The recent momentum in power engineering to incorporate green technology such as solar and wind power generation has sparked many such research process. Grid-forming converter technology is regarded as a promising tech to add such power generations while upholding the resiliency of the grid. This research thesis is providing a control scheme which serves as its backbone.

My first thanks goes to my Prof. Dominic Groß for providing me with the platform to work on this topic. Additionally this study would not have been possible without the the funding provided by Power System Engineering Research Council (PSERC). To conduct some of the additional studies we collaborated with Maryam Saeedifard and Zexian Zeng from Georgia Institute of Technology and hereby I would like to extend my thanks to them as well.

I am grateful for Dept of Electrical and Computer Engineering of University of Wisconsin Madison for providing an arena to demonstrate and hone our research abilities and all the staff how ensure a thriving environment. Ultimately, I would like to thank my parents, colleagues and friends for supporting me.

Abstract

In this study, we investigate grid-forming (GFM) control for dc/ac voltage source converters (VSC) under unbalanced system conditions and unbalanced faults. To fully leverage the degrees of freedom of VSCs, we introduce the concept of generalized three-phase GFM control that combines individual GFM controls for every phase with a phase balancing feedback. The proposed control allows trading off voltage and power unbalance under unbalanced conditions, enables current limiting for each phase during unbalanced faults, and reduces to positive sequence GFM droop control in balanced systems. High-fidelity simulations are used to illustrate the properties of the control and their interaction with protection schemes of distribution system.

1 Introduction

1.1 Motivation

Climate change is an ongoing crisis in our environment which is ubiquitously affecting our lives. A counter measure to mitigate this comes from reducing carbon emissions. Net-Zero by 2050, a mission overseen by Department of Energy, is a stride in this direction. Furthermore, the energy consumption is an ever increasing trend, which demands more energy production. To meet this sustainability goal, we need steep renewable power production integration. The majority of this renewable power is expected to be contributed by wind farms and solar energy, which are predominately connected onto the grid through power electronic circuits [3]. Collectively they are known as Inverter Based Resources (IBRs)

At present, Synchronous generators (SGs) are the backbone of the large scale power systems, and according to the DoE 40% of them are run from fossil fuels. Clean energy IBRs are though to replace most of these SGs and to fulfill the energy gap by 2050. But, decommissioning such SGs inhibits grid stability during contingencies and unbalanced loading, which are key indicators of grid resiliency. Standard IBR controls available in literature often overlook these nuance which can, jeopardize system reliability and resilience. This poses a significant barrier for large-scale integration of renewables and power electronics.

1.2 Literature review

There are two main control strategies for grid-connected power converters which are grid-following and grid-forming. Grid-following (GFL) converters may provide grid-supporting services but require other devices to form a stable ac voltage waveform that GFL converters can lock on to [4]. GFL converter mainly acts as current source (fig. 1.1) hence needs a phase locked loop (PLL) to inject power [4]. Typically, GFL converters shut off power during a large disturbance and reconnect only after the rest of the grid is restored. As IBR account for increasing shares of the overall electricity supply, GFL control strategies are impractical to employ on them [5]. Grid-forming (GFM) converters impose a well-defined and stable ac voltage waveform at their point of connection [1,2,6] and the active and reactive power delivered by the converter are function of ac grid frequency and voltage [4](fig.1.1). Depending on the type of control objective(for example droop, VSM, VOC etc) it is possible to mimic SGs inertial response to some extent. Additionally, this means that such converters can work in both grid-connected and islanded modes. Hence, GFM converters are envisioned to replace SGs as the foundation of future sustainable power systems [7,8]. Key advantages of GFM control include its

fast response to contingencies [8] and potential for fast fault current injection. However, these GFM converters are dc/ac voltage source converters and due to their comparatively low current limits, they cannot emulate the fault response of synchronous machines [9]. In contrast, SGs provide a fault response that is constrained solely by the electromechanical limits of SGs [3,10]. Consequently, the fault-response of a converter-dominated power system may vastly differ from the response expected by today’s system protection [11]. As mentioned previously, GFL converters leverage constant current injection to ride through faults [12]. But, the (self-synchronizing) voltage source characteristics of GFM converters are not amenable to this approach.

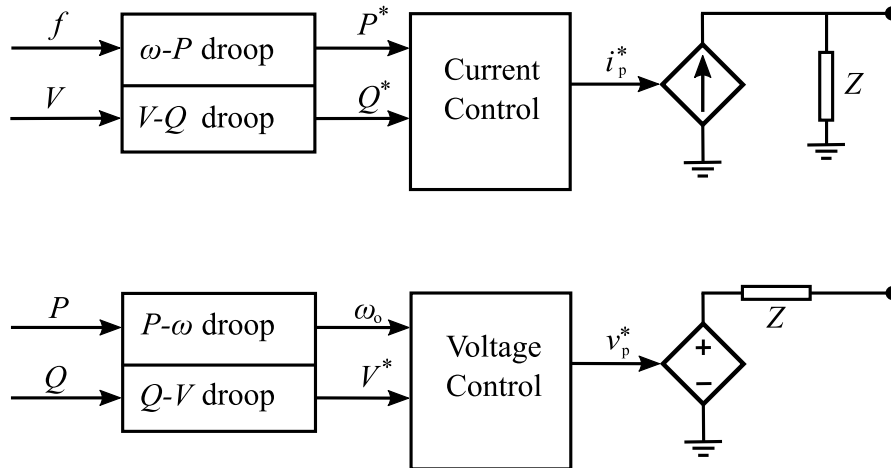


Figure 1.1: GFL converter acting as a current source (upper image), GFM converter acting as a voltage source (lower image).

Specifically, GFM controls provide a balanced voltage reference that is tracked by underlying cascaded voltage and current controllers. These loops control the dynamic behavior of the LCL filter at the terminal of the converter, hence enabling desirable voltage generation at the filter capacitor. Strategies for current limiting in GFM voltage source converters (VSCs) include limiting the reference of the inner current controller [9], virtual impedance [9,13,14], and projected droop control [15]. There is no control architecture in the literature at this time which allows GFM converters to simultaneously limit current and perfectly synthesis the grid. Nevertheless, GFM converters can ride through faults with certain current limiting control strategies. Crucially, all the aforementioned works assume a balanced system and balanced faults, the vast majority of faults in high voltage systems are unbalanced [16].

Moreover, distribution systems typically exhibit significant unbalance that is not accounted for in the standard GFM control design methods. The few works that consider GFM control under unbalanced conditions [17,18] and faults [18] typically leverage symmetrical components, e.g., implementing separate GFM controls for positive and negative sequence. This approach is motivated by prevailing analysis methods for unbalanced systems using symmetrical components and can effectively control the VSC terminal voltage under unbalanced conditions. However, the relationship between the

converter phase currents and symmetrical components is highly nonlinear [18] and limiting the phase currents through control of symmetrical components results in challenging control design and analysis problems. Instead, we propose explicitly controlling the phase voltages and currents in their original coordinates and apply droop control to each phase individually with a phase balancing feedback. This results in a less complex controller that can readily use standard current limiting algorithms and result in less complex control design problems and analysis problems.

The contribution of this work is a generalized three-phase GFM droop control for two-level dc/ac voltage source converters (VSCs) that leverages the capabilities of VSCs to control individual phase voltages and currents during unbalanced conditions and faults. To this end, single-phase GFM controls for every phase are combined with a phase balancing feedback. Using this approach, the GFM control can provide an unbalanced voltage reference under unbalanced conditions or unbalanced faults. Notably, the proposed control allows trading off voltage unbalance and power unbalance and reduces to standard balanced GFM droop control in balanced systems. The GFM voltage references are tracked by individual inner current and voltage controllers for every phase with phase current limiting. As a result, the proposed generalized GFM control sustains control over the VSC terminal voltage waveform under unbalanced conditions and phase currents under unbalanced faults. Finally, these features are illustrated using a high-fidelity EMT simulation.

1.3 Outline

This study outlooks the details on the control logic used to develop a novel three-phase grid-forming droop control. To explain this comprehensively we start with converter model settings and coordinate frame utilized in ch. 2 and ch. 3 respectively. Then, once we establish the hardware architecture, we elaborate on the converter control in ch. 4 and the measurement manipulations involved into achieving the desired voltage magnitude and angle at the filter capacitor in ch. 5. Furthermore, in ch. 6 we conduct steady state analysis to observe how the average active and reactive power steady state values differ under different settings. Ultimately, in ch. 7 we illustrate the theory discussed with case studies involving high fidelity simulations. For the concluding remarks we summarize the research conducted so far and shed light on the future work.

2 GFM converter setting

GFM converter is primarily composed of a VSC, dc source and filters with appropriate measurements for its functionality execution.

2.1 Topology

Representative power inverter topologies for utility-scale photovoltaic plants are two-level three-phase inverter, and three-level three-phase inverter and its variants. This is due to two-level and three-level VSCs being more suitable and cost-effective VSCs for low voltage or low power applications at the distribution level. While multi module converters can be easily scaled to higher power and voltages, it is too expensive for such low power applications. Besides being easier to implement compared to multi modular converters, they are very well understood. In this study we are making use of two-level three-phase dc/ac VSC to implement our GFM control.

2.2 Connection on the dc side

In this study, we are consistent with the standard GFM converter assumption that the dc side is an ideal source, which means that the GFM converter needs another device to stabilize the dc voltage or needs dc terminal to be an infinite dc bus. Accommodating dc voltage conditions into the overall control objective is out of scope for this study. Additionally, in our studies we have presumed the source is an ideal voltage source split in half where the split contact is connected to ground (mid point grounding scheme) as shown in fig. 2.1. This facilitates any zero sequence current to flow into the battery when present. Such arrangement is equivalent to having a midpoint of split capacitor grounded.

2.3 Filter configuration

Typically VSC are coupled with filter such as LCL or RLC to smoothen the voltage output waveform of two-level inverters and to subdue the harmonics the modulation may produce. In this study we have employed RLC circuit as our filter. Note that the filter topology is three-phase star connected where RL is connected in series to the output of the VSC and a capacitor is connected from the RL terminal to the neutral of the star connection as per the fig. 2.1. This neutral point is then connected with the midpoint ground of the dc side, hence closing the path for the zero current or flow.

We have chosen this arrangement of filter since the control demands each phase be controlled independently (sec. 3). The filter can also be connected in the Δ which then

allows the GFM control to reduce to a two-phase structure rather than a three-phase since one of the phases would be dependent on the other two phases. This logic eliminates the zero sequence current flow. Consequently, midpoint grounding at the dc side can be eliminated.

Filter can also be used to make the network more inductive as seen from the converter. This can be handy when the control logic is designed to work for inductive lines but the system is deployed in a slightly less inductive and more resistive network. $P - f$ and $Q - V$ droop equations work well only on the inductive network. Therefore by choosing a filter with higher inductance this relation can be preserved. But note that this may change the time scales of the dynamic response of the filter.

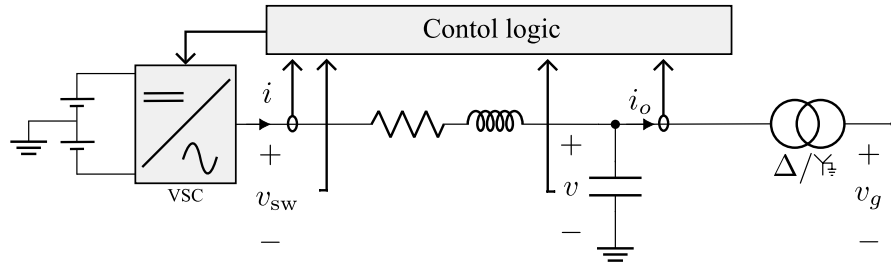


Figure 2.1: GFM converter consisting of 2-level VSC with mid point dc grounding. Note that the filter is in star configuration with its neutral point connected to ground. The Δ/Y transformer is used to connect GFM converter to grid.

2.4 Measurements

As per the Fig. 2.1 every control action GFM converter control logic takes is based on the reading sent from measurement sensors. To capture the optimal information on power flow and contingency, we use values of three-phase ac voltage $v_{sw} \in \mathbb{R}^3$ modulated by the VSC, filter current $i \in \mathbb{R}^3$, filter capacitor voltage $v \in \mathbb{R}^3$, and output current $i_o \in \mathbb{R}^3$. Sensors are placed accordingly to reduce the measurement error and external interference.

2.5 Transformer

The topology used in our study is Δ/Y transformer where Δ is on the primary side and the Y is on the secondary. This has to do with the arrangement of the filter. Since filter is star connected we kept Δ configuration on the primary side to avoid zero sequence current leakage into the rest of the system. Also it is essential to keep star connection on the secondary side with the solid grounding on the neutral to help ground any zero sequence fault current flow from the system. Depending on the filter (sec. 2.3) arrangement this transformer topology can be relaxed.

3 Coordinate frames

It is imperative to discuss the coordinate frame in which the measurement signals (sec. 2.4) are going to be fed into control logic. Although it is often presumed in literature that the signals are balanced, we will also look into the apt coordinate frame to be used if the signal is not balanced. Ultimately, the philosophy behind using right coordinate frame is to simplify calculations and consequently control logic.

3.1 Signals

Signals generated from the VSC or the ones captured from the measurements sensors are time based signals. They have a value for the given time stamp. Let signal $x(t) \in \mathbb{R}$ be the value at time $t \in \mathbb{R}$. If $x(t)$ is sinusoidal and oscillates at a constant time period with $\|x(t)\| := \hat{x}$ where $\|\cdot\|$ is euclidean norm, then considering the total time period as 2π rad, the value at any time stamp of the signal can be represented as \hat{x} at a phase angle θ where $\theta \in [0, 2\pi]$ rad. This is well known phasor representation which equivalently can be represented as $\hat{x}e^{j\theta} = \hat{x}(\cos \theta + j \sin \theta)$, where $j = \sqrt{-1}$.

3.2 $dq0$ coordinates for balanced systems

When the GFM converter is operating in balanced condition, i.e if the loading is uniform on all three-phases, then it is efficient to use $dq0$ transformation. This transformation is composed of Clarke and Park transformation. The Clarke transform is isolating that part of the vector which is common to all three phases of the vector and the Park transform rotates a vector's reference frame at an arbitrary frequency. Let $x_p(t) := \hat{x}_p \cos(\omega_p t + \theta_p)$ be a time domain ac signal of phase $p \in \mathcal{P}$ with amplitude $\hat{x}_p \in \mathbb{R}$, at time $t \in \mathbb{R}$. This signal has a constant frequency $\omega_p \in \mathbb{R}$ and phase difference $\theta_p \in \mathbb{R}$. For $\mathcal{P} := \{a, b, c\}$ we get,

$$\begin{bmatrix} x_d(t) \\ x_q(t) \\ x_0(t) \end{bmatrix} = \sqrt{\frac{2}{3}} \begin{bmatrix} \cos(\omega t) & \cos(\omega t - \frac{2\pi}{3}) & \cos(\omega t + \frac{2\pi}{3}) \\ -\sin(\omega t) & -\sin(\omega t - \frac{2\pi}{3}) & -\sin(\omega t + \frac{2\pi}{3}) \\ \frac{\sqrt{2}}{2} & \frac{\sqrt{2}}{2} & \frac{\sqrt{2}}{2} \end{bmatrix} \begin{bmatrix} x_a(t) \\ x_b(t) \\ x_c(t) \end{bmatrix}. \quad (3.1)$$

Here ω is an arbitrary frequency. The output $x_d(t)$ and $x_q(t)$ have a phase difference of $\pi/2$ rad. If all the phases are balanced, one of the inference from (3.1) is that $x_0(t)$ would be zero. Also, note that (3.1) modifies the time variant $x_a(t), x_b(t)$ and $x_c(t)$ signals into time invariant $x_d(t)$ and $x_q(t)$ signals, given that the former signals are sinusoidally changing at the frequency ω . If not, then $x_d(t), x_q(t)$ and $x_0(t)$ are time varying transformation of the input signal. It is important to point out that there are

studies which vastly makes use of $dq0$ transformation of the input signals to implement control logic for GFM converter [4]. This can be attributed to its simplified calculations and invariant nature of the variables involved to an extent. The 0 in $dq0$ is omitted because usually input signals in these systems are balanced.

3.3 Unbalanced systems

3.3.1 Symmetrical components

Unlike dq -transformation, the symmetrical components make use of the phasor $\hat{x}_p(\cos \theta_p + j \sin \theta_p) := \mathbf{x}_p$ where $p \in \mathcal{P}$. Symmetrical components for $\mathcal{P} := \{a, b, c\}$ can be represented as

$$\begin{bmatrix} \mathbf{x}_1 \\ \mathbf{x}_2 \\ \mathbf{x}_0 \end{bmatrix} = \frac{1}{3} \begin{bmatrix} 1 & 1 & 1 \\ 1 & \alpha & \alpha^2 \\ 1 & \alpha^2 & \alpha \end{bmatrix} \begin{bmatrix} \mathbf{x}_a \\ \mathbf{x}_b \\ \mathbf{x}_c \end{bmatrix}. \quad (3.2)$$

Here, $\alpha = e^{j\frac{2\pi}{3}}$, $\mathbf{x}_1, \mathbf{x}_2$ and \mathbf{x}_0 are positive, negative and zero sequence components of phasors $\mathbf{x}_a, \mathbf{x}_b$ and \mathbf{x}_c . This method is used to split the unbalanced phasors into the symmetric components. With balanced input signals, the negative and zero sequence components are null. Therefore the balanced signals can be then reduced back to their time domain signals which are inturn converted to dq -frame to be used in control logic. This kind of control logic is often called the positive sequence control, since the balanced input signals only consists of positive sequence components. In the cases where the signal is unbalanced then it is possible to convert the positive, negative and zero sequence signals separately into their corresponding dq -frame counterparts to be used in control logic. However, this sort of control is complicated to implement and execute because of its high non-linear nature (sec. 1.2). Besides, the symmetrical components needs input from phasors which is not always possible to accurately calculate in cases where the input frequency cannot be accurately determined which is true especially during faults.

3.3.2 Hilbert transform

Usage of the dq transformation is effective when applied to three phase systems for balanced grid conditions. However, during unbalanced cases, the signals produced by this transformation wont be constant, thus defeating its purpose. Nevertheless, the essence of these established control logic can be leveraged even in unbalanced scenarios. One such way is to apply these control logic to each phase separately and use the dq transformation for the phase wise measurement of signals.

Let $\omega_p \in \mathbb{R}$ denote the GFM reference voltage frequency for phase $p \in \mathcal{P}$. Then, for all $p \in \mathcal{P}$ and any ac signal $x_p(t)$, we estimate the quadrature component $x_p^\perp(t) \in \mathbb{R}$ of $x_p(t) \in \mathbb{R}$ as

$$x_p^\perp(t) := x_p(t - \frac{1}{4} \frac{1}{\omega_p(t)}). \quad (3.3)$$

In other words, under the assumption that $x_p(t)$ is a sinusoidal signal with slowly changing frequency $\omega_p(t)$, the time shifting in (3.3) referred to as Hilbert transform in the power electronics literature approximates a 90° phase shift. Notably, the Hilbert transform can be interpreted as representing $\alpha\beta$ components of an ac signal (i.e., $(x_{p,\alpha}, x_{p,\beta}) = (x_p, x_p^\perp)$). Let $R(\cdot)$ denote the 2D rotation matrix (Park transformation). Then, any ac signal $x_p(t)$ can be represented in a dq frame with reference angle $\theta_p(t) \in \mathbb{S}$ as

$$x_{p,dq}(t) := \begin{bmatrix} x_{p,d}(t) \\ x_{p,q}(t) \end{bmatrix} := R(\theta_p(t)) \begin{bmatrix} x_p(t) \\ x_p^\perp(t) \end{bmatrix}. \quad (3.4)$$

where $\frac{d}{dt}\theta_p(t)$ an arbitrary frequency. Moreover, for any ac signal $x_p(t)$ we can construct the phasor

$$\mathbf{x}_p(t) := x_{p,d}(t) + jx_{p,q}(t). \quad (3.5)$$

Since $\frac{d}{dt}\theta_p(t) = \omega_p(t)$, the output signals from (3.4) are dc signals which are invariant. Because of the modular implementation and better control logic associated with this method and, in this study we employ sec. 3.3.2 to convert all measurement signals into corresponding dq -frame signals.

4 Converter control

4.1 General tasks

The major idea behind developing the control strategy for this VSC is to match all the possible corresponding features an SG provides. To this end, we identified the following key control tasks for the GFM control to reproduce.

1. Voltage waveform - Impose a stable ac voltage waveform with tractable voltage amplitude and frequency. This is the crucial feature for a GFM converter to energize the system and to inject power. Additionally, it is beneficial for the system, if the GFM control contributes to voltage balancing during unbalanced loading.
2. Tracking - Asymptotically track a steady-state dispatch signal by a higher-level controller under nominal system conditions. With this GFM converter can precisely track filter voltage v , output current i_o and active and reactive power injected to take optimal control action.
3. Primary control - Autonomously respond to contingencies as well as variations in load and generation to stabilize the system. This acute feature can be attributed to maintaining the resiliency of the grid when incorporated in GFM control.
4. Protection - Operate within the VSC limits (e.g., current limit). Unlike SGs, converters are not electromechanical devices. Since each component used in VSC have their respective rated capacity, such as, rated current for FETs or IGBTs, the GFM control needs to protect VSC from crossing these hardware limitations.

These general tasks of the converter control is to replicate SG functionalities in almost every way except during faults, because of the hardware limitations of the VSCs. Meanwhile, also utilize the these VSC hardware to its optimal potential to control voltage magnitude and angle at each phase individually and swiftly.

To implement the above, we employ cascaded control technique where the above control tasks are achieved through cascading the response of inner control and outer control. Inner control provides the VSC immediate references to track. In our case, this provides the VSC the voltages magnitude and angle to follow as per 1st task. Furthermore, inner control helps VSC reduce the error in its output waveform by including the corrections necessary, as per the 2nd task. Outer control monitors the GFM converter to produce the necessary primary response as per the control objective which is responsible to execute 3rd task. Protection blocks are usually separate blocks which are used to limit the references passing from one block to other, making it certain that references provided do not exceed the rated capacity of the VSC hardware, hence serving 4th task. Such

cascaded control when deployed as a standard GFM control can be illustrated as per fig. 4.1

4.2 Standard (positive sequence) GFM control

The standard dual-loop GFM control architecture dispatches positive sequence voltage waveforms at the VSC terminal. The reference voltage magnitude $V^{\text{gfm}} \in \mathbb{R}$ and angle $\theta^{\text{gfm}} \in \mathbb{S}$ is generated from GFM control block which acts as outer control (sec. 4.1) depicted in fig. 4.1. Voltage magnitude reference V^{gfm} is then passed onto inner control which are voltage and current proportional-integral (PI) loops. They use dq -frame attached to the angle θ^{gfm} to track the reference provided. A current limit block is also utilized to limit the reference going into current control inner loop, which serves as a protection block against overcurrent. Also, it is not uncommon to see the use of virtual impedance to limit current instead of reference current limiting [13]. For the inner control, outer control and protection block to function and track the references precisely, the measurement signals v_{sw}, i, v and i_o for all three-phases are converted into their respective dq -frame phasors by using the same reference angle θ^{gfm} .

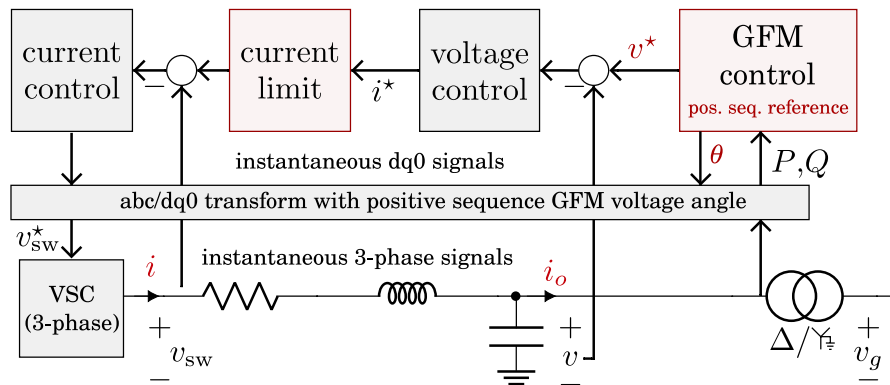


Figure 4.1: Standard dual-loop GFM control with inner controls tracking a positive sequence voltage reference provided by an outer GFM control (e.g., droop control [1], VSM [2]).

For a balanced system keeping the control blocks in dq -frame is much simpler (sec. 3.2, sec. 3.3.1). But as mentioned in sec. 1.2, most of the scenarios encountered in the system are unbalanced (be it loading or contingency), which renders this method inadequate. During severely unbalanced conditions such as faults, the VSC tries to impose balanced voltage at its terminals, which is not met. Consequently, this leads to higher current output from the VSC on the affected phase. This current is limited by the current saturation limiter block. When the converter is operating in the current saturation mode, the inner loops can no longer track the output voltage waveform at the capacitor of the converter which leads to the distorted waveform shown in the sec. 7.3.1. Therefore, using dq -frame in such scenarios may push the GFM control to produce response of a low output power quality.

To handel unbalanced cases reliably, in this study we propose generalized three-phase GFM control. This control structures enables three-phase voltage magnitude and frequency to be controlled separately for each phase and additionally opens a new set of possibilities of trade off between voltage and power unbalance (sec. 5.1).

5 Generalized three-phase GFM control

5.1 Control Overview

Tracking the voltage waveform in the best way is to track the individual phase quantities separately which is possible by using the inner loops for each phase. To this end, we need individual reference signals for each phase. This control structure of producing references and tracking them for each phase individually comes with an added benefit of additional degrees of freedom in the form of controlling voltage magnitude and angle for each phase. Figure 5.1 shows the generalized three-phase GFM control architecture proposed in this study that combines individual inner current and voltage controllers for every phase, individual outer GFM controls for every phase and a phase balancing feedback.

To enable control of individual phase currents and voltages, a reference frequency $\omega_p^{\text{gfm}} \in \mathbb{R}$, angle $\theta_p^{\text{gfm}} \in \mathbb{S}$ and voltage $V_p^{\text{gfm}} \in \mathbb{R}$ for every phase $p \in \mathcal{P}$ with $\mathcal{P} := \{a, b, c\}$ provided by the outer GFM control is used to estimate phasors for the phase voltages (sec. 3.3.2). Using these estimates, the inner voltage controller tracks the voltage reference phasors for every phase by calculating corresponding current reference. The resulting current reference for every phase is limited individually and tracked by individual inner current controller. We also discuss the implementation of virtual impedance instead of reference current limiting. Analogously to positive sequence GFM control, the gains of inner and outer loops need to be coordinated and chosen relative to the network circuit dynamics to ensure performance and stability [6, 19]. The outer GFM control combines GFM droop control for every phase with a phase balancing feedback that (i) ensures balanced references if the system is balanced, and (ii) allows trading off voltage and power unbalances under unbalanced conditions and faults. The inner and outer voltage control are in dq -frame for each phase individually.

5.2 Control description

In generalized three-phase GFM droop control the outer GFM control employs droop control [1] for individual phases, with phase balancing feedback. To attain that, outer control needs active and reactive power from each phase. Furthermore, the inner loops also need complete information on measurement signals of v_{sw}, i, v and i_o for each phase p . Using sec. 3.3.2 all the measurement signals are converted to their corresponding dq -frame counterparts, i.e for all $x_p(t) \in \{v_{sw,p}(t), i_p(t), v_p(t), i_{o,p}(t)\}$ the corresponding $x_p^\perp(t)$ where $p \in \mathcal{P}$ is obtained. For the voltage $v_p(t)$ and current $i_p(t)$ for each phase p , the average active power P_p and reactive power Q_p over one cycle can be computed using their corresponding current phasor $\mathbf{i}_p(t)$, voltage phasor $\mathbf{v}_p(t)$ and (5.6). Because

Here, $P_p^* \in \mathbb{R}$ and $Q_p^* \in \mathbb{R}$ are the active and reactive power setpoints and $\omega_0 \in \mathbb{R}_{>0}$ is the nominal frequency. Moreover, $\omega_p^{\text{gfm}} = \omega_0 + \frac{d}{dt} \delta_p^{\text{gfm}} \in \mathbb{R}$ is the GFM reference frequency for each phase $p \in \mathcal{P}$, $m_P \in \mathbb{R}_{>0}$ is the $P - f$ droop coefficient, $m_Q \in \mathbb{R}_{>0}$ is the $Q - V$ droop coefficient, $\tau \in \mathbb{R}_{>0}$ a lowpass filter time constant, and $k_P \in \mathbb{R}_{\geq 0}$ and $k_Q \in \mathbb{R}_{\geq 0}$ are the phase balancing feedback gains.

We emphasize that (5.7) reduces to three individual single-phase droop controls if $k_P = 0$, i.e., the GFM phase to neutral voltage frequency reference for each phase $p \in \mathcal{P}$ only depend on the active power measurements of phase $p \in \mathcal{P}$. In contrast, if $k_P > 0$, the phase balancing feedback trades off phase voltage frequency unbalance and deviations from the active power setpoints for each phase. Finally, for large k_P the phase voltage frequency balancing is stiff and the response of generalized three-phase droop control converges to the response of standard GFM droop control as $k_P \rightarrow \infty$. A block diagram of the GFM control (5.7) is shown in fig. 5.2a. Similar trend is observed when k_Q is varied where the effect is seen between phase voltage magnitude and reactive power illustrated in fig. 5.2b.

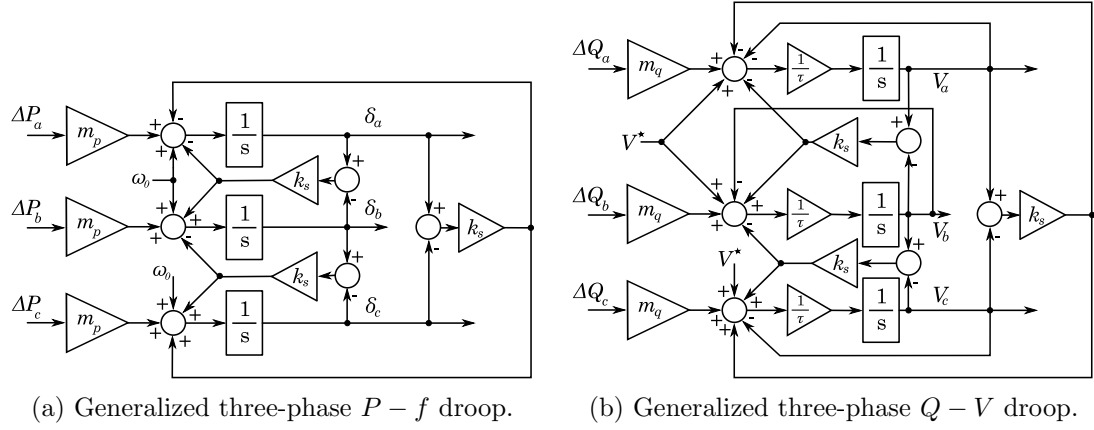


Figure 5.2: Droop control structure of generalized three-phase GFM control.

5.2.2 Dual-loop current/voltage control and current limiting

We implement voltage and current dual-loop proportional integral inner control to track the GFM voltage references provided by (5.7) for each phase (see fig. 5.1). To limit the current reference provided voltage control block is under the inverter current rating, we employ two main methods, notably current reference limiting and virtual impedance. The voltage controller can be realized as,

$$i_{p,dq}^{\text{ref}} = i_{o,p,dq} + Y_f v_{p,dq} + G_{\text{PI}}(s)(v_{p,dq}^{\text{gfm}} - v_{p,dq}), \quad (5.8)$$

with PI controller $G_{\text{PI}}(s)$, filter admittance matrix $Y_f \in \mathbb{R}^{2 \times 2}$, and voltage reference $v_{p,dq}^{\text{gfm}} \in \mathbb{R}^2$ (where $\|v_{p,dq}^{\text{gfm}}\| = V_p^{\text{gfm}}$ and $\angle v_{p,dq}^{\text{gfm}} = \theta_p^{\text{gfm}}$) compute the filter current reference

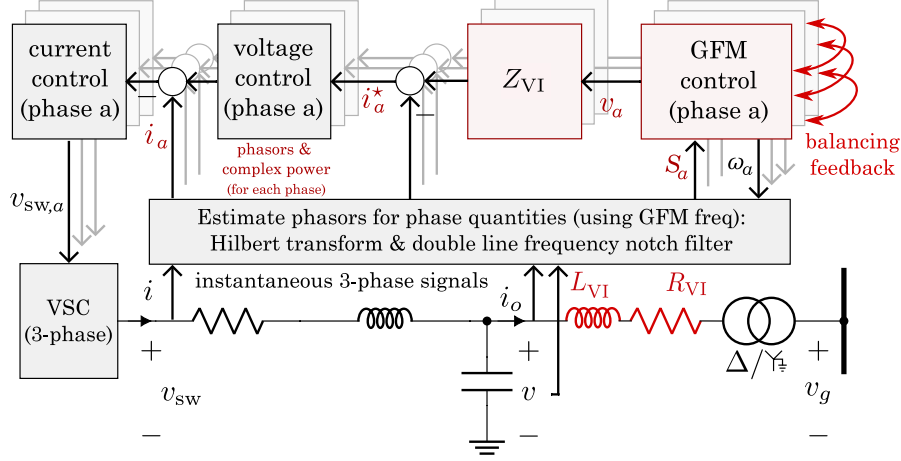


Figure 5.3: Virtual impedance $Z_{VI} := R_{VI} + j\omega_p^{\text{gfm}} L_{VI}$ in the GFM control structure and effective impedance emulation.

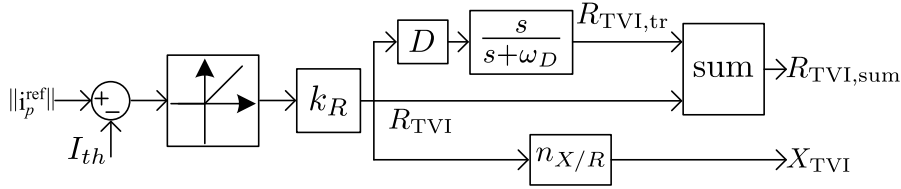


Figure 5.4: Virtual impedance activation and control structure.

$i_{p,dq}^{\text{ref}}$ for all $p \in \mathcal{P}$. Now, in the current reference limiting method, $i_{p,dq}^{\text{ref}}$ for phase $p \in \mathcal{P}$ is limited by,

$$\mathbf{i}_p^{\text{lim}} := \begin{cases} \mathbf{i}_p^{\text{ref}} & \text{if } \|\mathbf{i}_p^{\text{ref}}\| \leq I_{\text{max}} \\ i_{\text{max}} \angle \mathbf{i}_p^{\text{ref}} & \text{if } \|\mathbf{i}_p^{\text{ref}}\| > I_{\text{max}} \end{cases}, \quad (5.9)$$

where, $I_{\text{max}} \in \mathbb{R}_{>0}$ is maximum phase current magnitude for all phases individually. Hence, inner current control receives $\mathbf{i}_p^{\text{lim}}$ as the reference to track. Notably, unlike some commercial solutions, the current limiter (5.9) does not clip the current waveform, but adjusts the magnitude of the sinusoidal reference current for every phase to avoid introducing harmonics into the system

On the other hand, if virtual impedance is employed instead of reference current limiting then its effective implementation can be illustrated using fig. 5.3. The voltage drop across $Z_{VI} \in \mathbb{R}^2$ where $Z_{VI} := R_{VI} + j\omega_p^{\text{gfm}} L_{VI}$ indicated in the fig. 5.3 is

$$v_{p,dq,VI} = \begin{bmatrix} v_{p,d,VI} \\ v_{p,q,VI} \end{bmatrix}, \quad (5.10)$$

$$= \begin{bmatrix} R_{\text{TVI,sum}} & X_{\text{TVI}} \\ -X_{\text{TVI}} & R_{\text{TVI,sum}} \end{bmatrix} \begin{bmatrix} i_{o,p,d} \\ i_{o,p,q} \end{bmatrix}. \quad (5.11)$$

Here, as per the scheme suggested in [14], $R_{\text{TVI,sum}} \in \mathbb{R}_{>0}$ and $X_{\text{TVI}} \in \mathbb{R}_{>0}$ are determined based on the difference of $i_p^{\text{ref}} \in \mathbb{R}_{>0}$ and $I_{th} \in \mathbb{R}_{>0}$ as per fig. 5.4. Other parameters like $k_R \in \mathbb{R}_{>0}$ and $D \in \mathbb{R}_{>0}$ are determined by the X/R ratio $n_{X/R} \in \mathbb{R}_{>0}$, I_{max} and I_{th} . Voltage $v_{p,dq,\text{VI}} \in \mathbb{R}^2$ is subtracted from the voltage reference $v_{p,dq}^{\text{gfm}}$. Hence the reference passed onto inner current control is

$$i_{p,dq}^{\text{lim}} := i_{o,p,dq} + Y_f v_{p,dq} + G_{\text{PI}}(s)(v_{p,dq}^{\text{gfm}} - v_{p,dq,\text{VI}} - v_{p,dq}). \quad (5.12)$$

Finally, for each $p \in \mathcal{P}$ we use the inner current controller

$$v_{\text{sw},p,dq} = v_{p,dq} + Z_f i_{p,dq} + G_{\text{PI}}(s)(i_{p,dq}^{\text{lim}} - i_{p,dq}), \quad (5.13)$$

where $Z_f \in \mathbb{R}^{2 \times 2}$ denotes the filter impedance matrix and $v_{\text{sw},p,dq} \in \mathbb{R}^2$ is the phase voltage modulated by the VSC.

5.2.3 Discussion

The generalized three-phase droop control proposed in this section has three key features. First, the balancing gains k_P and k_Q adjust the trade-off between phase voltage frequency unbalance vs active power unbalance and phase voltage magnitude unbalance vs reactive power unbalance at the converter ac terminal. For example, k_P allows to adjust the contribution of a dc/ac VSC to mitigating angle unbalances in a distribution system. Second, even for large values of k_P/k_Q , a key feature of generalized three-phase droop control is that it (i) tracks voltage frequency/magnitude references for every phase, and (ii) can control and limit the phase currents individually through reference current limiter (5.9) or virtual impedance (5.12) (iii) the control explicitly addresses sub-cycle overcurrent by continuously estimating and controlling phase current phasors and limiting their magnitude. Finally, from a theoretical point of view, the proposed control reduces to standard GFM control if the system is balanced. Simulations performed to compare (positive sequence) performance and stability to standard GFM control only identified significant differences when using negligible phase-balancing gains k_P/k_Q .

6 Steady state analysis

6.1 Voltage magnitude and angle unbalances

In this section we illustrate how phase balancing gains and droop gains decide the stiffness in the voltage magnitude and angle balancing at the output terminals of the GFM converter. To make the notations less verbose we assign $V_{\delta,p}$ for $V_{\delta,p}^{\text{gfm}}$ and δ_p for δ_p^{gfm} for all $p \in \mathcal{P}$.

6.1.1 $Q - V$ droop equation

Generalized three-phase GFM droop equation for $Q - V$ droop is given by (5.7b). By expanding (5.7b) and by defining $Q_{\delta,p} := Q_p^* - Q_p$ where $p \in \mathcal{P}$, we have,

$$\tau \frac{d}{dt} \begin{bmatrix} V_{\delta,a} \\ V_{\delta,b} \\ V_{\delta,c} \end{bmatrix} = - \begin{bmatrix} V_{\delta,a} \\ V_{\delta,b} \\ V_{\delta,c} \end{bmatrix} - k_Q \underbrace{\begin{bmatrix} 2 & -1 & -1 \\ -1 & 2 & -1 \\ -1 & -1 & 2 \end{bmatrix}}_{:=L} \begin{bmatrix} V_{\delta,a} \\ V_{\delta,b} \\ V_{\delta,c} \end{bmatrix} + m_Q \begin{bmatrix} Q_{\delta,a} \\ Q_{\delta,b} \\ Q_{\delta,c} \end{bmatrix}. \quad (6.14)$$

Laplacian Matrix can be defined as L . Therefore,

$$\tau \frac{d}{dt} \begin{bmatrix} V_{\delta,a} \\ V_{\delta,b} \\ V_{\delta,c} \end{bmatrix} = -(I + k_Q L) \begin{bmatrix} V_{\delta,a} \\ V_{\delta,b} \\ V_{\delta,c} \end{bmatrix} + m_Q \begin{bmatrix} Q_{\delta,a} \\ Q_{\delta,b} \\ Q_{\delta,c} \end{bmatrix}, \quad (6.15)$$

$$\tau \frac{d}{dt} T \begin{bmatrix} V_{\delta,a} \\ V_{\delta,b} \\ V_{\delta,c} \end{bmatrix} = -T(I + k_Q L)T^{-1}T \begin{bmatrix} V_{\delta,a} \\ V_{\delta,b} \\ V_{\delta,c} \end{bmatrix} + m_Q T \begin{bmatrix} Q_{\delta,a} \\ Q_{\delta,b} \\ Q_{\delta,c} \end{bmatrix}. \quad (6.16)$$

Here, T is a transformation matrix defined as $T := \begin{bmatrix} \frac{1}{3} & \frac{1}{3} & \frac{1}{3} \\ 1 & -1 & 0 \\ 0 & 1 & -1 \end{bmatrix}$. Simplifying (6.16)

we get

$$\tau \frac{d}{dt} \begin{bmatrix} \bar{V}_\delta \\ V_{b-a} \\ V_{c-b} \end{bmatrix} = - \begin{bmatrix} 1 & 0 & 0 \\ 0 & 3k_Q + 1 & 0 \\ 0 & 0 & 3k_Q + 1 \end{bmatrix} \underbrace{\begin{bmatrix} \bar{V}_\delta \\ V_{b-a} \\ V_{c-b} \end{bmatrix}}_{=V_{\Delta,p}} + m_Q \begin{bmatrix} \bar{Q}_\delta \\ Q_{b-a} \\ Q_{c-b} \end{bmatrix}. \quad (6.17)$$

In (6.17), $V_{b-a} := V_{\delta,a} - V_{\delta,b} = V_a^* - V_a - (V_b^* - V_b)$, $Q_{b-a} := Q_{\delta,a} - Q_{\delta,b} = Q_a^* - Q_a - (Q_b^* - Q_b)$, $\bar{V}_\delta := \frac{1}{3} \sum_{p \in \mathcal{P}} V_{\delta,i}$ and $\bar{Q}_\delta := \frac{1}{3} \sum_{p \in \mathcal{P}} Q_{\delta,i}$. References such as V_p^* and Q_p^* are same $\forall p \in \mathcal{P}$ where $\mathcal{P} \in \{a, b, c\}$. Hence, we can simply write $V_{b-a} = V_b - V_a$ and $Q_{b-a} = Q_b - Q_a$. Looking closely at (6.17) we see that, the average voltage dynamics \bar{V}_δ

depend on the droop gain m_Q and average reactive power deviation \bar{Q}_δ . This behavior is holds true in positive sequence droop control discussed in sec. 4.2. Since it imposes balanced voltages on its terminal, the average voltage is similar to the per phase voltage and this depends on the reactive power injected and the droop gain. On the other hand, voltage magnitude difference between phases (not to be confused with line to line voltage) such as V_{b-a} is dependent on its corresponding reactive power magnitude difference such as Q_{b-a} and k_Q . To determine steady state response, we simply substitute $\frac{d}{dt}V_{\Delta,p} \rightarrow 0$ in (6.17). Hence we get

$$\begin{bmatrix} \bar{V}_\delta \\ V_{a-b} \\ V_{b-c} \end{bmatrix} = \begin{bmatrix} m_Q & 0 & 0 \\ 0 & -\frac{m_Q}{3k_Q+1} & 0 \\ 0 & 0 & -\frac{m_Q}{3k_Q+1} \end{bmatrix} \begin{bmatrix} \bar{Q}_\delta \\ Q_{a-b} \\ Q_{b-c} \end{bmatrix}. \quad (6.18)$$

It is evident form (6.18) that as $k_Q \rightarrow \infty$, $V_{a-b} \rightarrow 0$ suggesting that the phase voltages tend to be balanced.

6.1.2 $P - f$ droop equation

Similar arguments holds for Generalized three-phase GFM droop equation for $P - f$ given by (5.7b). By defining $P_{\delta,p} := P_p^* - P_p$ where $p \in \mathcal{P}$ and by expanding (5.7a) we get

$$\frac{d}{dt} \begin{bmatrix} \delta_a \\ \delta_b \\ \delta_c \end{bmatrix} = \omega_0 I - k_P \begin{bmatrix} 2 & -1 & -1 \\ -1 & 2 & -1 \\ -1 & -1 & 2 \end{bmatrix} \begin{bmatrix} \delta_a \\ \delta_b \\ \delta_c \end{bmatrix} + m_P \begin{bmatrix} P_{\delta,a} \\ P_{\delta,b} \\ P_{\delta,c} \end{bmatrix}. \quad (6.19)$$

By defining $\omega_{\delta,p} := \frac{d}{dt}\delta_p - \omega_0$, we have

$$\begin{bmatrix} \omega_{\delta,a} \\ \omega_{\delta,b} \\ \omega_{\delta,c} \end{bmatrix} = -k_P L \begin{bmatrix} \delta_a \\ \delta_b \\ \delta_c \end{bmatrix} + m_P \begin{bmatrix} P_{\delta,a} \\ P_{\delta,b} \\ P_{\delta,c} \end{bmatrix}, \quad (6.20)$$

$$T \begin{bmatrix} \omega_{\delta,a} \\ \omega_{\delta,b} \\ \omega_{\delta,c} \end{bmatrix} = -k_P T L T^{-1} T \begin{bmatrix} \delta_a \\ \delta_b \\ \delta_c \end{bmatrix} + m_P T \begin{bmatrix} P_{\delta,a} \\ P_{\delta,b} \\ P_{\delta,c} \end{bmatrix}. \quad (6.21)$$

Since, P_p^* is same $\forall p \in \mathcal{P}$ and by recalling §5.2.1, (6.21) reduces to

$$\begin{bmatrix} \bar{\omega}_\delta \\ \omega_{a-b} \\ \omega_{b-c} \end{bmatrix} = \begin{bmatrix} 0 & 0 & 0 \\ 0 & -3k_P & 0 \\ 0 & 0 & -3k_P \end{bmatrix} \begin{bmatrix} \bar{\delta} \\ \delta_{a-b} \\ \delta_{b-c} \end{bmatrix} + m_P \begin{bmatrix} \bar{P}_\delta \\ -P_{a-b} \\ -P_{b-c} \end{bmatrix}. \quad (6.22)$$

where, $\omega_{a-b} := \omega_a - \omega_b$, $P_{a-b} := P_a - P_b$, $\bar{\omega}_\delta := \frac{1}{3} \sum_{p \in \mathcal{P}} \omega_{\delta,i}$ and $\bar{P}_\delta := \frac{1}{3} \sum_{p \in \mathcal{P}} P_{\delta,i}$. Similar to $Q - V$ droop equation analysis, (6.22) shows that the average frequency deviation $\bar{\omega}_\delta$ is only dependent on average active power deviation \bar{P}_δ during steady state. The frequency difference between phases such as ω_{a-b} , however, is dependent on

its corresponding active power difference such as P_{a-b} . Since $\omega_{a-b} := \frac{d}{dt}\delta_{a-b}$, we have,

$$\frac{d}{dt}\delta_{a-b} = -3k_P\delta_{a-b} - m_P P_{a-b}, \quad (6.23a)$$

$$\delta_{a-b}(t) = e^{-3k_P t}\delta_{a-b}(0) - \frac{m_P}{3k_P}P_{a-b}(1 - e^{-3k_P t}). \quad (6.23b)$$

During steady state, i.e as $t \rightarrow \infty$, $e^{-3k_P t} \rightarrow 0$. Therefore,

$$\delta_{a-b}(t) = -\frac{m_P}{3k_P}P_{a-b}. \quad (6.24)$$

Same holds true for the solution of $\delta_{b-c}(t)$. Hence, we can simplify (6.22) as,

$$\bar{\omega}_\delta = m_P \bar{P}_\delta, \quad (6.25a)$$

$$\begin{bmatrix} \delta_{a-b} \\ \delta_{b-c} \end{bmatrix} = - \begin{bmatrix} \frac{m_P}{3k_P} & 0 \\ 0 & \frac{m_P}{3k_P} \end{bmatrix} \begin{bmatrix} P_{a-b} \\ P_{b-c} \end{bmatrix}. \quad (6.25b)$$

From (6.25b) it can be inferred that as $k_P \rightarrow \infty$, $\delta_{a-b} \rightarrow 0$ suggesting that the phase voltage angles tend to be balanced as well. Therefore along with sec. 6.1.1, when the balancing gains k_P and k_Q are high enough we can expect the voltage magnitude and angle to be similar to positive sequence droop control counterpart.

6.2 Unbalance factors

Let V^+ and V^- denote magnitude of the positive and negative sequence voltage and let $\bar{P} := \frac{1}{3} \sum_{p \in \mathcal{P}} P_p$ and $\bar{Q} := \frac{1}{3} \sum_{p \in \mathcal{P}} Q_p$ denote the average phase power of the VSC. The standard voltage unbalance factor is given by $V_{UF} := V^-/V^+$. Moreover, for P_p and Q_p in p.u., we define the power unbalance factors $P_{UF} := \max_{p \in \mathcal{P}} |P_p - \bar{P}|$, and $Q_{UF} := \max_{p \in \mathcal{P}} |Q_p - \bar{Q}|$ that resemble standard current unbalance factors for electric machines. In this section we want to demonstrate that for a given system with GFM converter, it is possible to bound the voltage unbalance factor V_{UF} of the GFM converter with the given information of unbalance factors of the system.

6.2.1 Linearizing voltage unbalance factor

Since V_{UF} is a highly non-linear function with respect to V_p and θ_p we are linearizing it at a balanced operating point. To this end, we use 2nd order Taylor series expansion. For $p \in \mathcal{P}$,

$$\begin{bmatrix} V^+ \\ V^- \\ V^0 \end{bmatrix} = \frac{1}{3} \begin{bmatrix} 1 & 1 & 1 \\ 1 & \alpha & \alpha^2 \\ 1 & \alpha^2 & \alpha \end{bmatrix} \begin{bmatrix} V_a e^{j\theta_a} \\ V_b e^{j\theta_b} \\ V_c e^{j\theta_c} \end{bmatrix} \quad (6.26)$$

$$V_{UF}^2 = \frac{(V^-)^2}{(V^+)^2} \quad (6.27)$$

$$= f(x) \quad (6.28)$$

where $x = (\delta_a, \delta_b, \delta_c, V_a, V_b, V_c)$ and $f : \mathbb{R}^6 \rightarrow \mathbb{R}$. Also recall from the sec. 5.2.1 that $\delta_p = \theta_p - \theta_p^{\text{bal}}$. For $\gamma \in (0, 1)$, Taylor 2nd order expansion is given by

$$f(y) = f(x_0) + \langle \nabla f(x_0), y - x_0 \rangle + \frac{1}{2}(y - x_0)^\top \nabla^2 f(x_0 + \gamma(y - x_0))(y - x_0). \quad (6.29)$$

For $x_0 = \begin{bmatrix} 1_3 \\ 0_3 \end{bmatrix}$, we get $f(x_0) = 0$ and $\nabla f(x_0) = \mathbb{0}_6$. Hence we have

$$f(y) = \frac{1}{2}(y - x_0)^\top \nabla^2 f(x_0 + \gamma(y - x_0))(y - x_0). \quad (6.30)$$

Now, we can omit the constant $\frac{1}{2}$ and mark the right hand side as an upper bound. Therefore,

$$f(y) \leq (y - x_0)^\top \nabla^2 f(x_0)(y - x_0). \quad (6.31)$$

Still the the domain of the f is in 6th dimension. Making an attempt to reduce it we use coordinate transformation same as sec. 6.1.1. Let $\tilde{T} := \begin{bmatrix} T & 0_{3 \times 3} \\ 0_{3 \times 3} & T \end{bmatrix}$. Also, let $\tilde{x} := \tilde{T}x$. Then, $\tilde{T}^{-1}\tilde{x} = x$. Substituting in (6.31) we get

$$f(y) \leq (\Delta x)^\top (\tilde{T}^{-1})^\top \nabla^2 f(x_0) \tilde{T}^{-1} \Delta x, \quad (6.32)$$

where $\Delta x = \tilde{T}(y - x_0)$. From the (6.32), simplifying $H := (\tilde{T}^{-1})^\top \nabla^2 f(x_0) \tilde{T}^{-1}$ we obtain,

$$H = \begin{bmatrix} 0 & 0 & 0 & 0 & 0 & 0 \\ 0 & \frac{2}{9} & -\frac{1}{9} & 0 & 0 & \frac{\sqrt{3}}{9} \\ 0 & -\frac{1}{9} & \frac{2}{9} & 0 & -\frac{\sqrt{3}}{9} & 0 \\ 0 & 0 & 0 & 0 & 0 & 0 \\ 0 & 0 & -\frac{\sqrt{3}}{9} & 0 & \frac{2}{9} & -\frac{1}{9} \\ 0 & \frac{\sqrt{3}}{9} & 0 & 0 & -\frac{1}{9} & \frac{2}{9} \end{bmatrix}. \quad (6.33)$$

Also, note that $\Delta x = (\bar{\delta}, \delta_{a-b}, \delta_{b-c}, \bar{V}, V_{a-b}, V_{b-c})$. In (6.33), the corresponding elements of Δx where the columns of H are zero can be omitted. Consequently the H can also be shrunk. This is supported by the intuition that average values don't affect the unbalance factor. Hence,

$$\tilde{H} := \begin{bmatrix} \frac{2}{9} & -\frac{1}{9} & 0 & \frac{\sqrt{3}}{9} \\ -\frac{1}{9} & \frac{2}{9} & -\frac{\sqrt{3}}{9} & 0 \\ 0 & -\frac{\sqrt{3}}{9} & \frac{2}{9} & -\frac{1}{9} \\ \frac{\sqrt{3}}{9} & 0 & -\frac{1}{9} & \frac{2}{9} \end{bmatrix}, \quad (6.34)$$

$$(6.35)$$

and $\Delta \tilde{x} := (\delta_{a-b}, \delta_{b-c}, V_{a-b}, V_{b-c})$. Substituting \tilde{H} and $\Delta \tilde{x}$ in (6.31), we get

$$V_{UF}^2 \leq (\Delta \tilde{x})^\top \tilde{H} \Delta \tilde{x}. \quad (6.36)$$

Summarizing, (6.36) is linearized version of V_{UF}^2 near the balanced operating point of x_0 with reduced dimension of the state vector from \mathbb{R}^6 to \mathbb{R}^4 with the help of coordinate transformation \tilde{T} .

6.2.2 Standalone GFM converter with unbalanced load

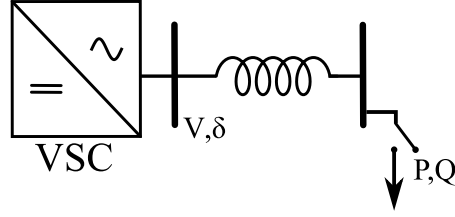


Figure 6.1: VSC of GFM converter is connected to an unbalanced load.

When the GFM converter is connected to the load which is drawing unbalanced powers as depicted in fig. 6.1, the corresponding voltage magnitude and angle unbalance is captured through through (6.18) and (6.22). Using (6.36) and recalling the relationship between active power and power angle given in (6.25b) and reactive power and voltage given in (6.18) we get

$$V_{UF}^2 \leq \begin{bmatrix} P_{a-b} \\ P_{b-c} \\ Q_{a-b} \\ Q_{b-c} \end{bmatrix}^T \begin{bmatrix} \frac{m_P}{3k_P} & 0 & 0 & 0 \\ 0 & \frac{m_P}{3k_P} & 0 & 0 \\ 0 & 0 & \frac{m_Q}{3k_Q+1} & 0 \\ 0 & 0 & 0 & \frac{m_Q}{3k_Q+1} \end{bmatrix}^T \tilde{H} \begin{bmatrix} \frac{m_P}{3k_P} & 0 & 0 & 0 \\ 0 & \frac{m_P}{3k_P} & 0 & 0 \\ 0 & 0 & \frac{m_Q}{3k_Q+1} & 0 \\ 0 & 0 & 0 & \frac{m_Q}{3k_Q+1} \end{bmatrix} \begin{bmatrix} P_{a-b} \\ P_{b-c} \\ Q_{a-b} \\ Q_{b-c} \end{bmatrix}, \quad (6.37)$$

$$\leq \begin{bmatrix} P_{a-b} \\ P_{b-c} \\ Q_{a-b} \\ Q_{b-c} \end{bmatrix}^T \begin{bmatrix} \frac{2m_P^2}{81k_P^2} & -\frac{m_P^2}{81k_P^2} & 0 & \frac{\sqrt{3}m_P m_Q}{27k_P(3k_Q+1)} \\ -\frac{m_P^2}{81k_P^2} & \frac{2m_P^2}{81k_P^2} & -\frac{\sqrt{3}m_P m_Q}{27k_P(3k_Q+1)} & 0 \\ 0 & -\frac{\sqrt{3}m_P m_Q}{27k_P(3k_Q+1)} & \frac{2m_Q^2}{9(3k_Q+1)^2} & -\frac{m_Q^2}{9(3k_Q+1)^2} \\ \frac{\sqrt{3}m_P m_Q}{27k_P(3k_Q+1)} & 0 & -\frac{m_Q^2}{9(3k_Q+1)^2} & \frac{2m_Q^2}{9(3k_Q+1)^2} \end{bmatrix} \begin{bmatrix} P_{a-b} \\ P_{b-c} \\ Q_{a-b} \\ Q_{b-c} \end{bmatrix}. \quad (6.38)$$

Let,

$$\gamma_1 := \frac{m_P^2}{81k_P^2} [P_{a-b} \ P_{b-c}] \begin{bmatrix} 2 & -1 \\ -1 & 2 \end{bmatrix} \begin{bmatrix} P_{a-b} \\ P_{b-c} \end{bmatrix}, \quad (6.39)$$

$$\gamma_2 := \frac{m_Q^2}{(3k_Q+1)^2} [Q_{a-b} \ Q_{b-c}] \begin{bmatrix} 2 & -1 \\ -1 & 2 \end{bmatrix} \begin{bmatrix} Q_{a-b} \\ Q_{b-c} \end{bmatrix}, \quad (6.40)$$

$$\gamma_3 := \frac{2\sqrt{3}m_P m_Q}{27k_P(3k_Q+1)} [Q_{a-b} \ Q_{b-c}] \begin{bmatrix} 0 & -1 \\ 1 & 0 \end{bmatrix} \begin{bmatrix} P_{a-b} \\ P_{b-c} \end{bmatrix}. \quad (6.41)$$

Then, (6.38) can be equivalently be represented as,

$$V_{UF}^2 \leq \gamma_1 + \gamma_2 + \gamma_3. \quad (6.42)$$

The objective is to maximize the (6.42) to determine the upper bound on V_{UF}^2 .

Since, the power imbalances are bounded by their respective power unbalance factors, they serve as the constraints for the optimization problem. Recalling the definition of P_{UF} and Q_{UF} ,

$$P_{UF} \geq \frac{1}{3} \begin{bmatrix} 2 & -1 & -1 \\ -1 & 2 & -1 \\ -1 & -1 & 2 \\ -2 & 1 & 1 \\ 1 & -2 & 1 \\ 1 & 1 & -2 \end{bmatrix} \begin{bmatrix} P_a \\ P_b \\ P_c \end{bmatrix}, \quad (6.43)$$

$$\geq \frac{1}{3} \begin{bmatrix} 2 & -1 & -1 \\ -1 & 2 & -1 \\ -1 & -1 & 2 \\ -2 & 1 & 1 \\ 1 & -2 & 1 \\ 1 & 1 & -2 \end{bmatrix} T^{-1} \begin{bmatrix} \bar{P} \\ P_{a-b} \\ P_{b-c} \end{bmatrix}, \quad (6.44)$$

$$\geq \frac{1}{3} \begin{bmatrix} 0 & 1 & 1 \\ 0 & -2 & 1 \\ 0 & 1 & -2 \\ 0 & -1 & -1 \\ 0 & 2 & -1 \\ 0 & -1 & 2 \end{bmatrix} \begin{bmatrix} \bar{P} \\ P_{a-b} \\ P_{b-c} \end{bmatrix}. \quad (6.45)$$

By removing the average element out of (6.45) we get

$$P_{UF} \geq \frac{1}{3} \begin{bmatrix} 1 & 1 \\ -2 & 1 \\ 1 & -2 \\ -1 & -1 \\ 2 & -1 \\ -1 & 2 \end{bmatrix} \begin{bmatrix} P_{a-b} \\ P_{b-c} \end{bmatrix}. \quad (6.46)$$

Reactive power unbalance power factor is also represented similarly by

$$Q_{UF} \geq \frac{1}{3} \begin{bmatrix} 1 & 1 \\ -2 & 1 \\ 1 & -2 \\ -1 & -1 \\ 2 & -1 \\ -1 & 2 \end{bmatrix} \begin{bmatrix} Q_{a-b} \\ Q_{b-c} \end{bmatrix}. \quad (6.47)$$

The constraint set (6.46) can be plotted as shown in fig. 6.2a for $P_{UF} = 0.5$. By observation the constraints can be simplified and over-approximated as shown in fig. 6.2b. Through equations, the simplified constraint set given in fig. 6.2b can be realized as

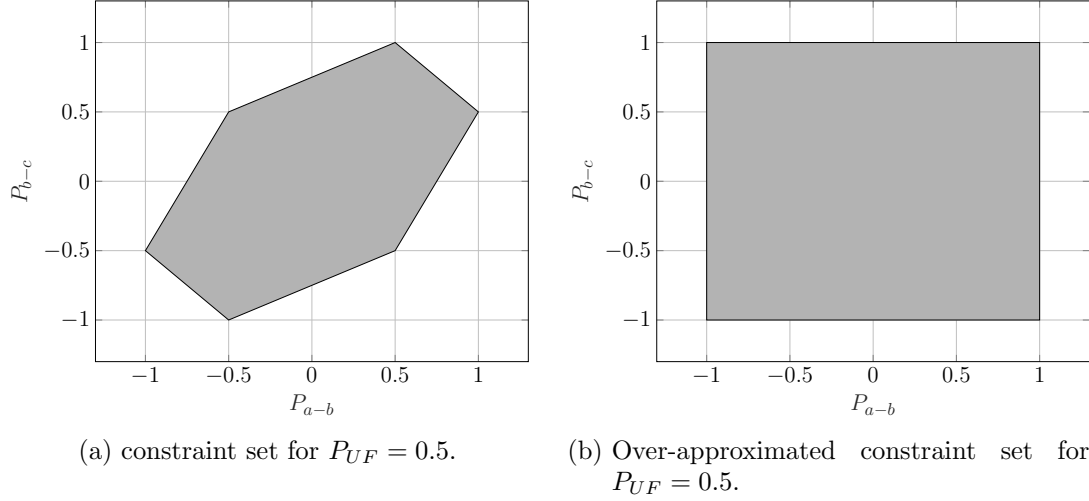


Figure 6.2: Constraint sets for the maximization of voltage unbalance factor.

$$P_{UF} \geq \frac{1}{2} \begin{bmatrix} 1 & 0 \\ 0 & 1 \\ -1 & 0 \\ 0 & -1 \end{bmatrix} \begin{bmatrix} P_{a-b} \\ P_{b-c} \end{bmatrix}. \quad (6.48)$$

Similar procedure can be performed to simplify the constraint set (6.47) which leads to,

$$Q_{UF} \geq \frac{1}{2} \begin{bmatrix} 1 & 0 \\ 0 & 1 \\ -1 & 0 \\ 0 & -1 \end{bmatrix} \begin{bmatrix} Q_{a-b} \\ Q_{b-c} \end{bmatrix} \quad (6.49)$$

For quick identification let us define constraint set given in (6.46) and (6.47) which is indicated in fig. 6.2a as \mathcal{X} and the set given in the (6.48) and (6.49) indicated in fig. 6.2b as $\tilde{\mathcal{X}}$. Then, the optimization problem can be represented as

$$\max_{x \in \mathcal{X}} (\gamma_1 + \gamma_2 + \gamma_3). \quad (6.50)$$

The upper bound on the optimization problem (6.50) can be written as,

$$\max_{x \in \mathcal{X}} \gamma_1 + \max_{x \in \mathcal{X}} \gamma_2 + \max_{x \in \mathcal{X}} \gamma_3. \quad (6.51)$$

For the optimization problem with objective function γ_1 and γ_2 and the constraint set \mathcal{X} , there exists a straight forward solution, since the number of variables in each of these problems are only two. However, the solution is complicated to achieve with objective function γ_3 and the constraint set \mathcal{X} , since the number of variables in the optimization problem raises to four. To arrive at the solution faster we can use the fact that $\mathcal{X} \leq \tilde{\mathcal{X}}$. Hence we get

$$\max_{x \in \mathcal{X}} \gamma_3 \leq \max_{x \in \tilde{\mathcal{X}}} \gamma_3. \quad (6.52)$$

Therefore, the upper bound on the (6.51) can be obtained as

$$\max_{x \in \mathcal{X}} \gamma_1 + \max_{x \in \mathcal{X}} \gamma_2 + \max_{x \in \mathcal{X}} \gamma_3. \quad (6.53)$$

The solution to the optimization problem given in (6.53) is given by

$$V_{UF}^2 \leq \frac{2m_P^2}{27k_P^2} P_{UF}^2 + \frac{2m_Q^2}{3(3k_Q + 1)^2} Q_{UF}^2 + \frac{16\sqrt{3}m_P m_Q}{27k_Q(3k_Q + 1)} P_{UF} Q_{UF}. \quad (6.54)$$

This bounds the voltage unbalance factor of the GFM converter through power unbalance factors of the load in a standalone GFM converter with an unbalanced load system.

6.2.3 GFM converter connected to unbalanced grid

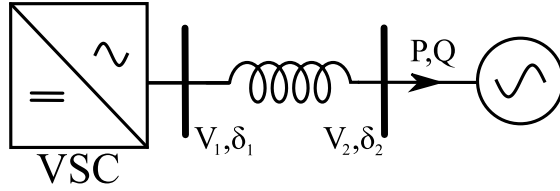


Figure 6.3: VSC of GFM converter is connected to an unbalanced load.

It is an interesting case to bound the voltage unbalance factor of the GFM converter with the voltage unbalance factor of the unbalance grid. Since the power pushed from the converter is a function of the voltage magnitude and the angle of the grid, there is an expectation to achieve the voltage unbalance factor bound on the GFM converter through the given value of voltage unbalance factor of the grid. As per the system given in fig. 6.3,

$$\begin{bmatrix} V_{1,a-b} \\ V_{1,b-c} \end{bmatrix} = - \begin{bmatrix} \frac{m_Q}{3k_Q+1} & 0 \\ 0 & \frac{m_Q}{3k_Q+1} \end{bmatrix} \begin{bmatrix} Q_{a-b} \\ Q_{b-c} \end{bmatrix}, \quad (6.55)$$

$$\begin{bmatrix} \delta_{1,a-b} \\ \delta_{1,b-c} \end{bmatrix} = - \begin{bmatrix} \frac{m_P}{3k_P} & 0 \\ 0 & \frac{m_P}{3k_P} \end{bmatrix} \begin{bmatrix} P_{a-b} \\ P_{b-c} \end{bmatrix}. \quad (6.56)$$

By linearizing reactive power near nominal point V^* and δ^* we get

$$\begin{bmatrix} V_{1,a-b} \\ V_{1,b-c} \end{bmatrix} = - \begin{bmatrix} \frac{m_Q}{3k_Q+1} & 0 \\ 0 & \frac{m_Q}{3k_Q+1} \end{bmatrix} \begin{bmatrix} b(V_{1,a-b} - V_{2,a-b}) \\ b(V_{1,b-c} - V_{2,b-c}) \end{bmatrix}, \quad (6.57)$$

$$\begin{bmatrix} V_{1,a-b} \\ V_{1,b-c} \end{bmatrix} = \begin{bmatrix} \frac{bm_Q}{3k_Q+bm_Q+1} & 0 \\ 0 & \frac{bm_Q}{3k_Q+bm_Q+1} \end{bmatrix} \begin{bmatrix} V_{2,a-b} \\ V_{2,b-c} \end{bmatrix}. \quad (6.58)$$

Similarly by linearizing active power we obtain,

$$\begin{bmatrix} \delta_{1,a-b} \\ \delta_{1,b-c} \end{bmatrix} = - \begin{bmatrix} \frac{m_P}{3k_P} & 0 \\ 0 & \frac{m_P}{3k_P} \end{bmatrix} \begin{bmatrix} b(\delta_{1,a-b} - \delta_{2,a-b}) \\ b(\delta_{1,b-c} - \delta_{2,b-c}) \end{bmatrix}, \quad (6.59)$$

$$\begin{bmatrix} \delta_{1,a-b} \\ \delta_{1,b-c} \end{bmatrix} = \begin{bmatrix} \frac{bm_P}{3k_P+bm_P} & 0 \\ 0 & \frac{bm_P}{3k_P+bm_P} \end{bmatrix} \begin{bmatrix} \delta_{2,a-b} \\ \delta_{2,b-c} \end{bmatrix}. \quad (6.60)$$

Combining (6.58) and (6.60) we get,

$$\begin{bmatrix} \delta_{1,a-b} \\ \delta_{1,b-c} \\ V_{1,a-b} \\ V_{1,b-c} \end{bmatrix} = F \begin{bmatrix} \delta_{2,a-b} \\ \delta_{2,b-c} \\ V_{2,a-b} \\ V_{2,b-c} \end{bmatrix}, F := \begin{bmatrix} \frac{bm_P}{3k_P+bm_P} & 0 & 0 & 0 \\ 0 & \frac{bm_P}{3k_P+bm_P} & 0 & 0 \\ 0 & 0 & \frac{bm_Q}{3k_Q+bm_Q+1} & 0 \\ 0 & 0 & 0 & \frac{bm_Q}{3k_Q+bm_Q+1} \end{bmatrix}. \quad (6.61)$$

Using (6.61) to bound the voltage unbalance factor, we get,

$$V_{1,UF}^2 \leq z_2^T \tilde{H}_F z_2, \quad (6.62)$$

where,

$$\tilde{H}_F := F^T \tilde{H} F, z_2 := \begin{bmatrix} \delta_{2,a-b} \\ \delta_{2,b-c} \\ V_{2,a-b} \\ V_{2,b-c} \end{bmatrix}. \quad (6.63)$$

For a given value of $V_{2,UF}$ we have

$$V_{2,UF}^2 = cz_2^T \tilde{H} z_2, c \in \mathbb{R}. \quad (6.64)$$

In a case where $z_2 \in \mathcal{N}(\tilde{H})$, $V_{2,UF}^2 = 0$. In such cases if the $z_2 \notin \mathcal{N}(\tilde{H}_F)$ then $V_{1,UF}^2 \neq 0$ which means that the GFM voltage unbalance factor bounds cannot be determined with the given grid voltage unbalance factor. On the other hand, if $z_2 \in \mathcal{N}(\tilde{H}_F)$ then $V_{1,UF}^2 = 0$. This also means that \tilde{H} and \tilde{H}_F have the same null space. One such way to force them to have the same null space is when all the element in F are same. This is true when,

$$\frac{bm_Q}{3k_Q + bm_Q + 1} = \frac{bm_P}{3k_P + bm_P}. \quad (6.65)$$

Hence, only in the cases where $\mathcal{N}(\tilde{H}) = \mathcal{N}(\tilde{H}_F)$ (where $\mathcal{N}(\cdot)$ is null space of a matrix), the bounds on the GFM voltage unbalance factor becomes,

$$V_{1,UF}^2 \leq \frac{1}{c} \left(\frac{bm_P}{3k_P + bm_P} \right)^2 V_{2,UF}^2. \quad (6.66)$$

Equation (6.66) is bounding the voltage unbalance factor of the GFM converter through voltage unbalance factor of the unbalanced grid.

7 Case study

Description	Value
Phase balancing gain k_P	1e5 p.u.
Phase balancing gain k_Q	1e5 p.u.
Phase balancing gain $k_P = k_Q := k_s$	1e5 p.u.
Inverter base power S_b	1e6 W
Inverter base voltage V_b	480 V
Inverter filter capacitor	0.05 p.u.
Inverter filter inductor	0.1 p.u.
Inverter filter resistor	0.01 p.u.
Inverter active power set point per phase	0.1 p.u.
Inverter reactive power set point per phase	0 p.u.
Inverter voltage set point per phase	1 p.u.
Threshold current limit I_{th}	1 p.u.
Absolute current limit I_{max}	1.2 p.u.
TVI constant k_R	0.817
TVI constant D	15.66
TVI constant $n_{X/R}$	5
TVI HPF cut-off frequency ω_D	100 Hz
$P - f$ droop m_P	0.05 p.u.
$Q - V$ droop m_Q	0.05 p.u.
Base frequency ω_0	$2\pi 60$ rad/s
Time constant τ	$\frac{10}{\omega_0}$ s
Medium voltage line resistance	0.21 Ω /km
Medium voltage line inductance	17e-4 H/km
Medium voltage line capacitance	1e-8 F/km
Medium voltage line base voltage	4.16e3 V
Medium voltage line length	1 km
High voltage line resistance	0.03 Ω /km
High voltage line inductance	7.95e-4 H/km
High voltage line capacitance	10e-9 F/km
High voltage line base voltage	230e3
High voltage line length	10

Table 7.1: Parameters used in the model illustrated in fig. 7.1

7.1 System description

To illustrate the results, we use a high-fidelity EMT simulation of a two-level dc/ac VSC connected to an infinite bus through a 1 km medium voltage line, a 40 km double circuit high voltage transmission line, and step up transformers. The system parameters are tabulated in Table. 7.1 and the control is implemented at a sampling rate of 10 kHz.

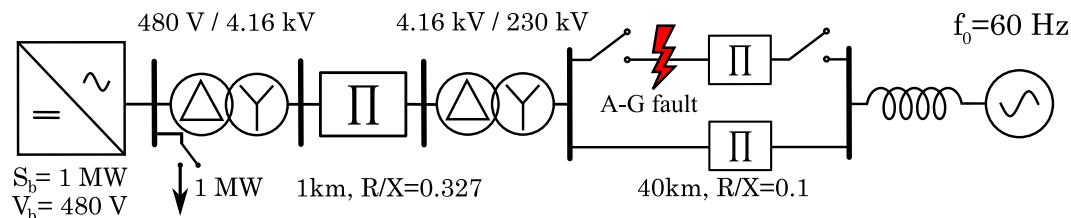


Figure 7.1: Test system with a low-voltage VSC connected to a weak ac system through a distribution line, double circuit transmission line, and a step up transformer.

From sec. 2.5 we can recall that the Δ side is connected to the inverter and the *Wye* side is connected to the rest of the system. The unbalanced load of 1MW cumulative is placed at the bus where inverter is attached for the inverter to closely observe the load unbalance. The fault is simulated on the upper transmission line among the double transmission line due to the breaker presence on its either side. Lastly the system is connected to infinite bus through an impedance which has an arbitrarily controlled short circuit ratio (SCR).

7.2 Unbalanced load

To illustrate the role of the phase balancing gain k_P and k_Q , fig 7.2 shows the steady-state voltage and power unbalance factors at the VSC terminal for an unbalanced delta connected constant impedance load¹ at the VSC bus (see fig. 7.1). The results show the expected trade off between voltage unbalance and power unbalance, i.e., increasing the phase balancing gain $k_P = k_Q := k_s$ reduces voltage unbalance V_{UF} but increases power unbalance P_{UF} and Q_{UF} .

This is evident from the equations (6.18) and (6.25b) which is analytically obtained from steady state analysis. As k_Q increases, the voltage imbalance between the phases reduces irrespective of the reactive power imbalance. Similarly, as k_P increase the angle difference between different phases also abets irrespective of the active power difference.

7.3 Single line-to-ground fault

To illustrate the impact of separate voltage/current control and current limiting for every phase on unbalanced fault ride through, we disconnect the load at the VSC terminal and

¹Relative to the load between phase *a* and *b*, the load between phase *b* and *c* is 20% lower and the load between phase *a* and *c* is 20% higher

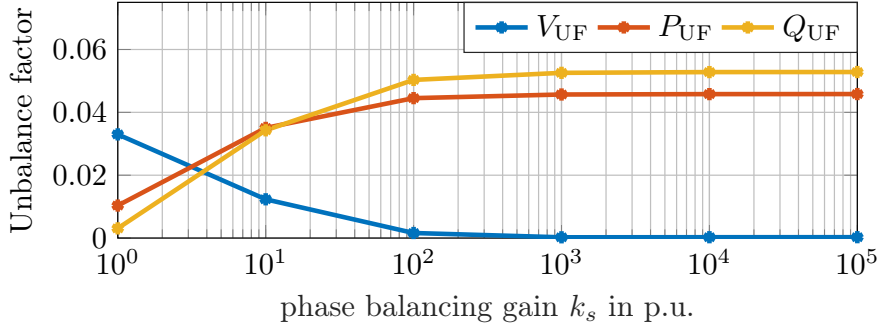


Figure 7.2: Steady-state unbalance factors for an unbalanced load at the VSC terminal and various phase balancing gains k_s .

consider a zero impedance line-to-ground fault for phase a of a transmission line (see fig. 7.1). Figure. 7.5 and fig. 7.7 show the resulting VSC terminal voltage magnitude $V_p = \|\mathbf{v}_p\|$, VSC phase current magnitude $I_p = \|\mathbf{i}_p\|$, active power P_p , and reactive power Q_p for every phase $p \in \mathcal{P}$. Because the magnitudes of phase currents and voltages are not well-defined within a cycle, the maximum magnitude over one cycle is shown. We use $k_s = 10^5$ p.u., i.e., the outer GFM control is configured to resemble standard droop control (sec. 4.2), and the fault is applied at $t = 1.5$ s and cleared after ten cycles by disconnecting the faulted line. Notably, due to the transformer connection, the fault applied to phase a of the transmission line, is effectively mapped to phase b at the VSC terminal.

7.3.1 Current saturation algorithm (CSA)

It can be seen that the current reference limiter (5.9) and PI current control (5.13) successfully limits the current magnitude to $I_{\max} = 1.2$ p.u. within each cycle. Notably, by controlling the current phasor for every phase, the proposed control explicitly handles sub-cycle overcurrent. Once the fault is cleared a significant resynchronization transient is observed that can be attributed to controller windup in the voltage loop (5.8) and GFM angle dynamics (5.7a).

To further illustrate the positive impact of the generalized three-phase GFM control, the simulation study has been repeated with standard droop control using the dual-loop inner control structure. In this case, the current and voltage waveforms are severely distorted because the VSC aims to impose balanced phase currents and a balanced voltage at its terminal. However, under its current limits, the VSC cannot maintain a balanced voltage at the terminal during the unbalanced fault. Terminal voltage waveforms for both controls are shown in fig. 7.3. It can be seen that the proposed control successfully imposes a sinusoidal ac voltage waveform at the terminals of the VSC that is unbalanced to limit the current. In contrast, standard droop control results in a highly distorted voltage. The reason for this distortion lies in dq transformations of such distorted waveform agreeing with the output voltage generated by the converter. In such cases the dq transformation alone is not sufficient to distinguish if the waveform generated is actu-

ally sinusoidal. On the other hand dq transformation applied to each phase individually produces finer waveform since the control structure has better visibility on the signals generated and also the means to correct it in a much finer level (by controlling voltage magnitude and angle instantaneously) which results in the smoother waveform.

Once the fault is removed it is observed that system returns to normal state but the power dispatch per phase of the GFM converter is slightly off from the power set-point. Considering 5% deviation of the power set-point per phase as an unstable response we captured the critical clearing time of the fault for the GFM converter operated at different values of phase balancing gain k_s . While doing so, we also varied the SCR value of the grid to observe the trend of critical clearing time from weak grid to strong grid, where higher SCR means stronger grid and lower SCR means weaker grid. Figure. 7.4 shows that as k_s increases the critical clearing time reduces. This sheds light on the limitation of standard GFM control since the with higher value of k_s the voltage balancing gets more stiffer. Additionally, as SCR increases the critical clearing time increases due to strength of the grid aiding in the fault recovery. The vertical axis is critical clearing time mentioned in terms of ac cycles at nominal frequency.

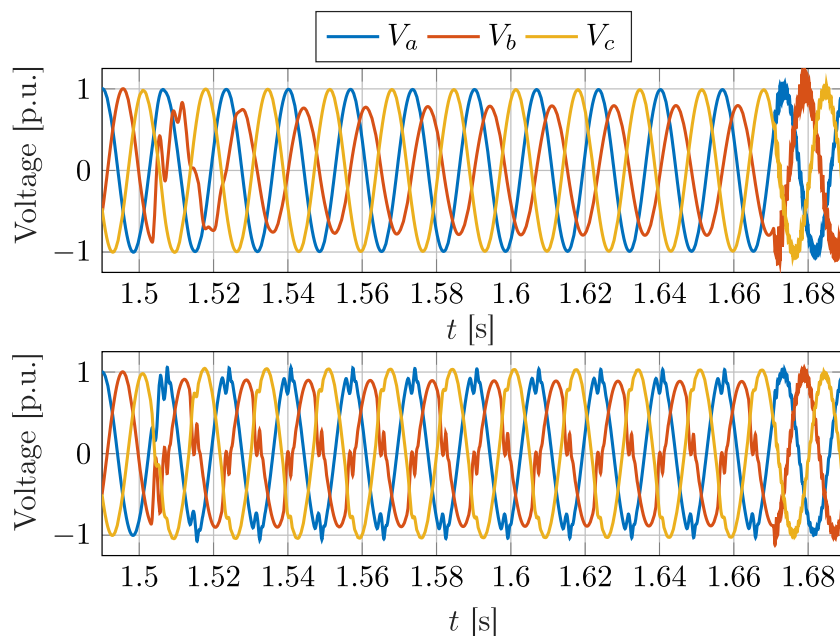


Figure 7.3: VSC voltages during a phase a to ground fault using generalized three-phase droop control with dual-loop current/voltage control for every phase (top) and standard droop control and dual-loop current/voltage control (bottom).

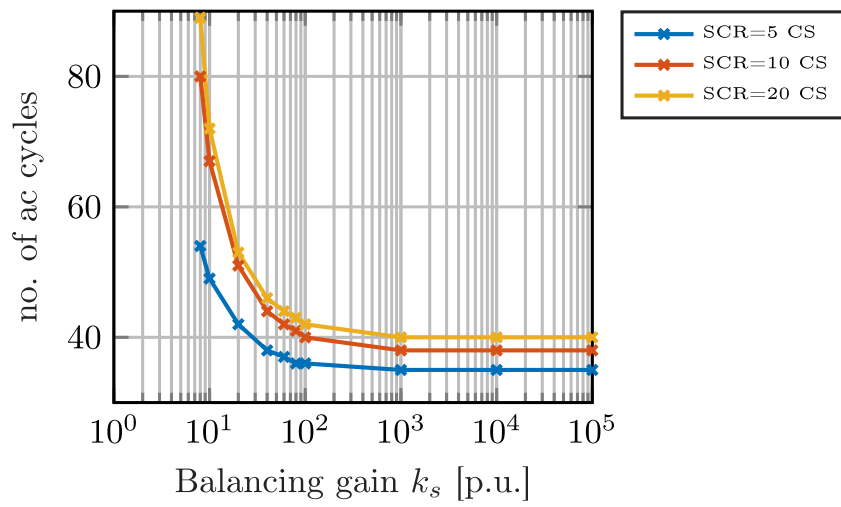


Figure 7.4: Critical clearing time vs phase balancing gain k_s for different SCR values. The vertical axis is critical clearing time mentioned in terms of ac cycles at nominal frequency.

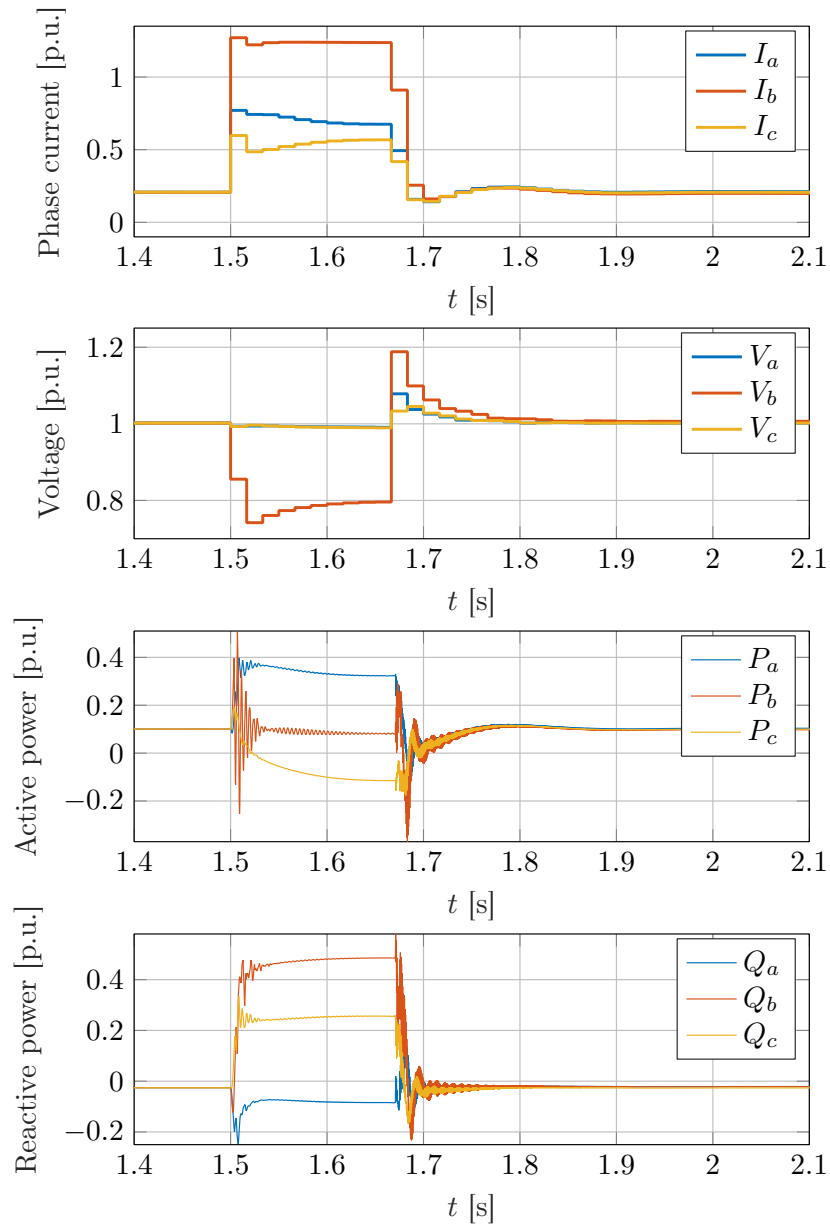


Figure 7.5: Response of generalized droop control to a phase a to ground fault on a transmission line at $t = 1.5$ s with CSA current limiting. The fault is cleared after ten cycles by disconnecting the faulted line.

7.3.2 Threshold virtual impedance (TVI)

The TVI is implemented as per (5.10) per phase individually²ft:gtech. The response of the GFM converter is captured in the fig. 7.1 when A-G fault is applied at the fault location. It is notable from fig. 7.7 that the fault current is limited more aggressively compared to that of CSA and consequently the voltage overshoot after the fault is removed is also lower. As the downside, the power, both active and reactive, are more distorted and noisy. Nevertheless, TVI provides an improved fault ride through response. One more advantage of using TVI is that it has shown to have longer critical clearing durations, at least many times than that observed in CSA method.

Notice how in both fig. 7.5 and fig. 7.7 after the fault is removed at $t = 1.67$ s there is an exponentially decaying ringing in the inverter response. We wanted to measure, which combination among SCR, current limiting method among CSA and TVI and phase balancing gain values allowed the GFM to come to its nominal operating conditions quicker. To this end, we recorded the duration from the time the fault is removed to the time the response is less than 5% deviant from its nominal value. Figure. 7.6 shows that while there is no obvious trend of resynchronization time with respect to SCR and current limiting method, it is definitely reducing with the increase in phase balancing gain k_s . Therefore, along with the tradeoff between the power and voltage imbalance, k_P and k_Q also help in trading off between resynchronization time and critical clearing time provided CSA current limiting method is used.

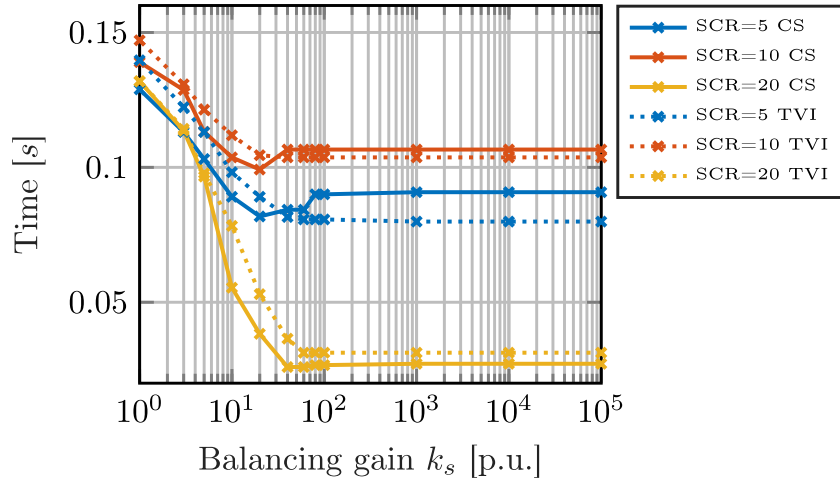


Figure 7.6: Resynchronization time vs phase balancing gain k_s . Dotted lines employ TVI for current limiting while solid lines employ CSA.

²This study was conducted with the help of Maryam Saeedifard and zexian Zeng from Georgia institute of technology

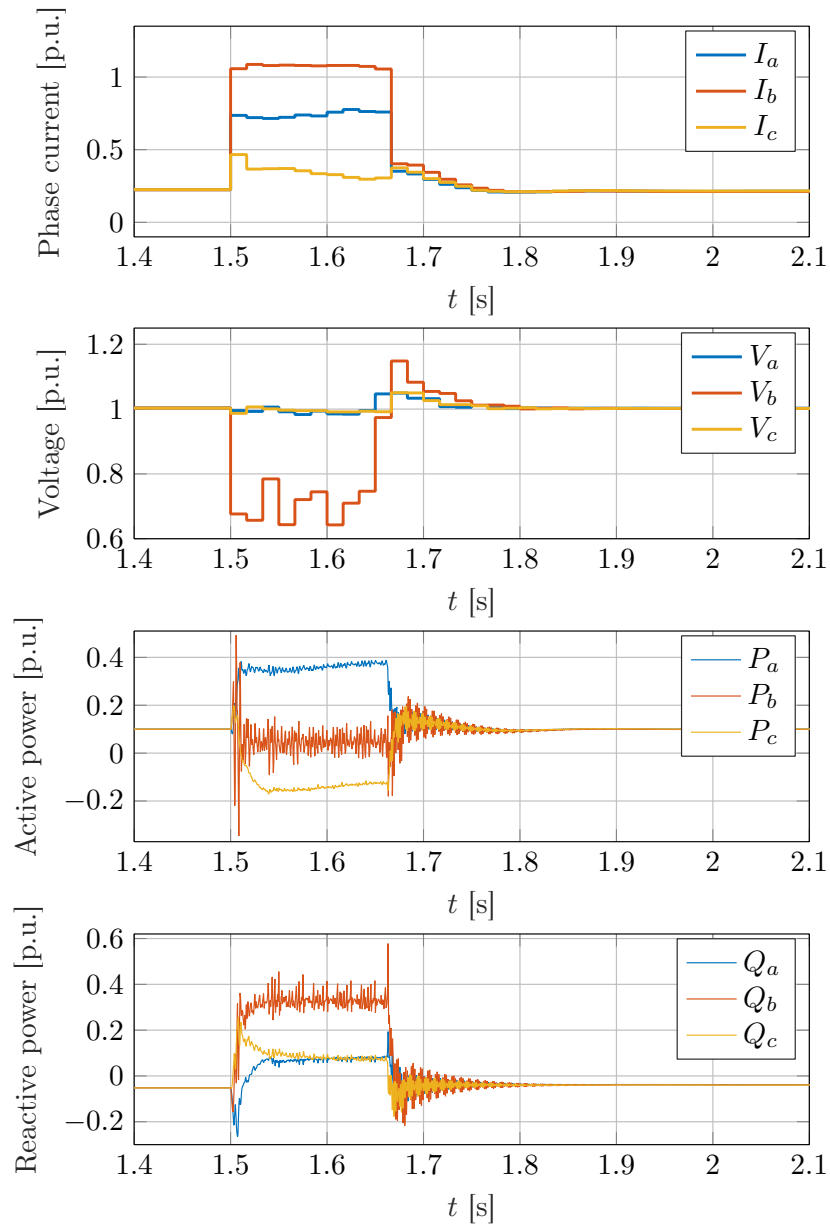


Figure 7.7: Response of generalized droop control to a phase a to ground fault on a transmission line at $t = 1.5$ s, with TVI current limiting. The fault is cleared after ten cycles by disconnecting the faulted line.

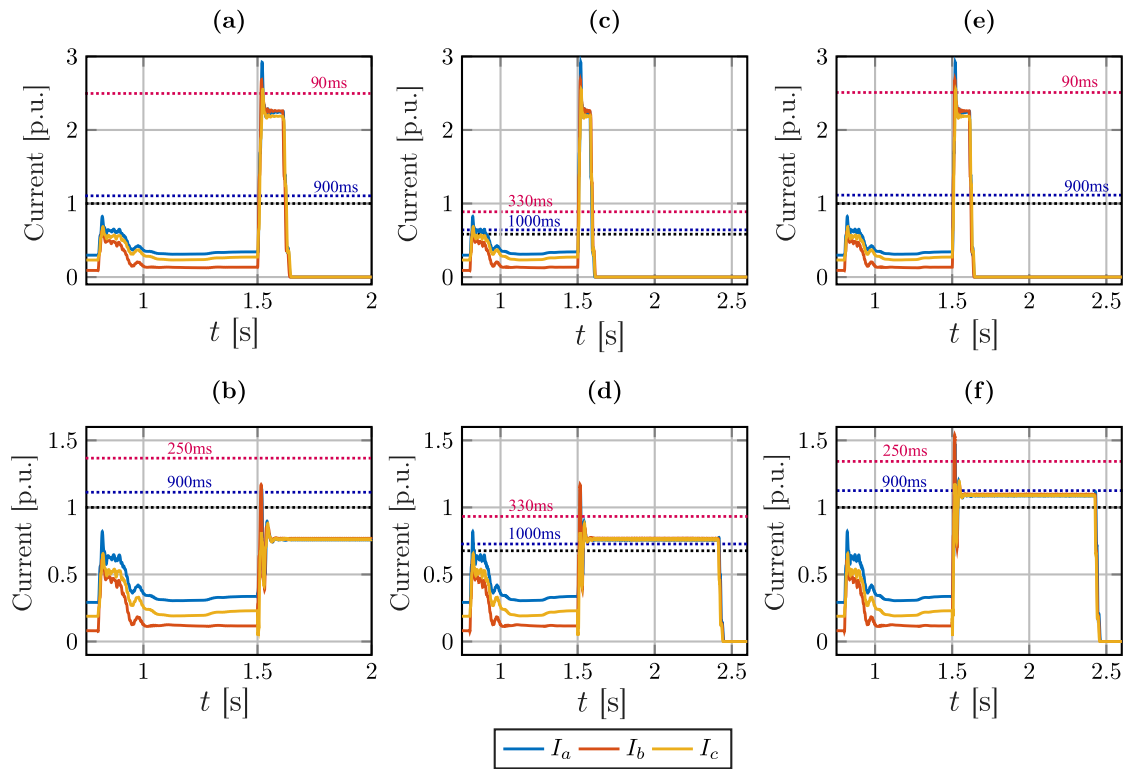


Figure 7.9: ABC-g fault with inverse time relay. Graphs (a) (c) (e) indicate the response of Relay 1 and graphs (b) (d) (f) indicate the response of Relay 2 as per fig. 7.8.

8 Conclusion

This study considered grid-forming control for three-phase dc/ac voltage source converters under unbalanced conditions and faults. In this context, we proposed a novel generalized three-phase droop control that combines individual GFM controls for every phase with phase balancing feedbacks. This generalized GFM control fully leverages the degrees of freedom of the VSC and allows trading off voltage and power unbalance under unbalanced conditions and reduces to standard droop control in balanced systems. Moreover, the voltage references generated by the outer GFM controls are tracked by inner dual-loop current and voltage controls for each phase that enable direct limiting of phase currents without clipping the current waveforms through major current limiting methods in literature. In contrast to standard GFM controls, this approach maintains full control of the VSC terminal voltage during unbalanced faults and enables effective limiting of phase currents during unbalanced faults. A high-fidelity case study is used to demonstrate the effectiveness of the proposed control under unbalanced low voltage loads and unbalanced faults and interactions of GFM control with legacy protection systems.

Bibliography

- [1] M. Chandorkar, D. Divan, and R. Adapa, “Control of parallel connected inverters in standalone ac supply systems,” *IEEE Trans. Ind. Appl.*, vol. 29, no. 1, pp. 136–143, 1993.
- [2] S. D’Arco, J. A. Suul, and O. B. Fosso, “A virtual synchronous machine implementation for distributed control of power converters in smartgrids,” *Electr. Power Sys. Res.*, vol. 122, pp. 180–197, 2015.
- [3] B. Kroposki, B. Johnson, Y. Zhang, V. Gevorgian, P. Denholm, B.-M. Hodge, and B. Hannegan, “Achieving a 100% renewable grid: Operating electric power systems with extremely high levels of variable renewable energy,” *IEEE Power Energy Mag.*, vol. 15, no. 2, pp. 61–73, 2017.
- [4] J. Rocabert, A. Luna, F. Blaabjerg, and P. Rodríguez, “Control of power converters in ac microgrids,” *IEEE Trans. Power Electron.*, vol. 27, no. 11, pp. 4734–4749, 2012.
- [5] U.S. Department of Energy, “Powering grid-forming inverters,” 2022. [Online]. Available: <https://www.energy.gov/eere/solar/articles/powering-grid-forming-inverters>
- [6] D. Groß, M. Colombino, J.-S. Brouillon, and F. Dörfler, “The effect of transmission-line dynamics on grid-forming dispatchable virtual oscillator control,” *IEEE Trans. Control Netw. Syst.*, vol. 6, no. 3, pp. 1148–1160, 2019.
- [7] J. Matevosyan, B. Badrzadeh, T. Prevost, E. Quitmann, D. Ramasubramanian, H. Urdal, S. Achilles, J. MacDowell, S. H. Huang, V. Vital, J. O’Sullivan, and R. Quint, “Grid-forming inverters: Are they the key for high renewable penetration?” *IEEE Power Energy Mag.*, vol. 17, no. 6, pp. 89–98, 2019.
- [8] A. Crivellaro, A. Tayyebi, C. Gavriluta, D. Groß, A. Anta, F. Kupzog, and F. Dörfler, “Beyond low-inertia systems: Massive integration of grid-forming power converters in transmission grids,” in *IEEE Power & Energy Society General Meeting*, 2020.
- [9] T. Qoria, F. Gruson, F. Colas, X. Kestelyn, and X. Guillaud, “Current limiting algorithms and transient stability analysis of grid-forming VSCs,” *Electr. Power Sys. Res.*, vol. 189, p. 106726, 2020.
- [10] E. Nasr-Azadani, C. A. Cañizares, D. E. Olivares, and K. Bhattacharya, “Stability analysis of unbalanced distribution systems with synchronous machine and dfig

- based distributed generators,” *IEEE Trans. Smart Grid*, vol. 5, no. 5, pp. 2326–2338, 2014.
- [11] J. Jia, G. Yang, A. H. Nielsen, and P. Rønne-Hansen, “Impact of VSC control strategies and incorporation of synchronous condensers on distance protection under unbalanced faults,” *IEEE Trans. Ind. Electron.*, vol. 66, no. 2, pp. 1108–1118, 2019.
- [12] J. Jia, G. Yang, and A. H. Nielsen, “A review on grid-connected converter control for short-circuit power provision under grid unbalanced faults,” *IEEE Trans. Power Del.*, vol. 33, no. 2, pp. 649–661, 2018.
- [13] A. D. Paquette and D. M. Divan, “Virtual impedance current limiting for inverters in microgrids with synchronous generators,” *IEEE Trans. Ind. Appl.*, vol. 51, no. 2, pp. 1630–1638, 2015.
- [14] Q. Taoufik, H. Wu, X. Wang, and I. Colak, “Variable virtual impedance-based overcurrent protection for grid-forming inverters: Small-signal, large-signal analysis and improvement,” *IEEE Trans. Smart Grid*, 2022.
- [15] D. Groß and F. Dörfler, “Projected grid-forming control for current-limiting of power converters,” in *Allerton Conference on Communication, Control, and Computing*, 2019, pp. 326–333.
- [16] IEEE Power System Relaying Committee Working Group, “Single phase tripping and auto reclosing of transmission lines,” *IEEE Trans. Power Del.*, vol. 7, no. 1, pp. 182–192, 1992.
- [17] E. Avdiaj, J. A. Suul, S. D’Arco, and L. Piegari, “A virtual synchronous machine-based control for eliminating DC-side power oscillations of three-phase VSCs under unbalanced grid voltages,” in *Int. Conference on Compatibility, Power Electronics and Power Engineering*, 2021.
- [18] M. A. Awal, M. R. K. Rachi, H. Yu, I. Husain, and S. Lukic, “Double synchronous unified virtual oscillator control for asymmetrical fault ride-through in grid-forming voltage source converters,” *IEEE Trans. Power Electron.*, 2022.
- [19] T. Qoria, F. Gruson, F. Colas, X. Guillaud, M.-S. Debry, and T. Prevost, “Tuning of cascaded controllers for robust grid-forming voltage source converter,” in *Power Systems Computation Conference*, 2018.